Minimal thermal modeling of two-way thermomechanically coupled plates for nonlinear dynamics investigation

Minimal thermal modelling of two-way thermomechanically coupled plates for nonlinear dynamics investigation

by Eduardo Saetta[1], Valeria Settimi[1], Giuseppe Rega[1]*

[1] *Department of Structural and Geotechnical Engineering, Sapienza University of Rome, Italy*
*Corresponding author: giuseppe.rega@uniroma1.it

Minimal thermal modelling of two-way thermomechanically coupled plates for nonlinear dynamics investigation

Eduardo Saetta, Valeria Settimi and Giuseppe Rega

Department of Structural and Geotechnical Engineering, Sapienza University of Rome, Rome, Italy

Abstract: Minimal thermal modelling of two-way thermomechanically coupled plates is addressed in the framework of a unified formulation of the underlying continuum problem. Variably refined reduced-order models are considered, and some main features of the relevant transient and steady responses to a variety of active thermal sources are investigated, by properly reconstructing 3D temperature configurations and energy balances. In comparison with a richer reduced model and available analytical solutions, a model with assumed cubic temperature distribution along the thickness has the advantage of being the minimal one still allowing to consider a wide set of boundary and body thermal excitations, while showing a comprehensive capability to reliably describe the thermal response. This appears of particular interest also in view of further pursuing a systematic, yet computationally demanding, investigation of the nonlinear dynamics of the coupled plate, in the cheapest possible way from both the mechanical and thermal viewpoint.

***Keywords*:** Composite plates, unified thermomechanical coupling, reduced-order models, thermal modelling, transient/steady response, global dynamics.

1. Introduction

Thermoelastic analysis of structures in a nonlinear dynamics environment is important for aerospace, civil and micro-electro-mechanical applications. Traditionally, it has been addressed via a solely one-way (from thermal to mechanical) approach in which the full thermomechanical interaction is overlooked, and the temperature distribution is assumed a priori, or obtained through the solution of the heat conduction equation, and considered just as an additional excitation in the forced mechanical equations to be solved subsequently. Using either low-dimensional models or models with a high number of degrees-of freedom also possibly validated by experimental tests, a meaningful variety of interesting results has been obtained as regards the influence of temperature on typical features of the nonlinear response of, e.g., beams [1-4] and plates [5-11], such as resonance curves, bifurcation scenarios, chaos occurrence, and mode involvement due to nonlinear and thermal couplings.

The one-way approach relies on the reasonable assumption that the thermal dynamics evolves over a much slower time-scale than the structural dynamics, so that the former affects the latter but not vice versa. Due to such a slow nature of temperature evolution, structural dynamics equations are modelled with a constant or averaged temperature over a given structural time span, and reduced-order models (ROMs) based on vibration modes of the unheated structure are constructed, even though the need of using a time-dependent basis of modes accounting for the even slow temperature variation has been highlighted, as well [12,13]. The last issue is comprehensively addressed in a recent study [14] in which a multiple time scale-based approach is used to solve the temperature-dependent structural dynamics equations by accounting for the coexisting slow/fast thermal/mechanical settings.

In contrast, fully coupled vibration analyses take into account the actual thermomechanical interaction entailed by the presence of displacement and temperature field variables in both mechanical and thermal

equations. Two-way coupling (from thermal to mechanical, and from mechanical to thermal) has been considered both experimentally and numerically in the analysis of dynamic effects caused by impact loading in inelastic monolithic materials [15-18], up to the recent development of a three-dimensional (3D) multiscale approach for the prediction of dynamic response of composite materials based on the generalized method of cells micromechanics theory [19]. For structural elements with linear elastic constituents, actual thermomechanical coupling under quasi-static or dynamic loading has been considered in several investigations conducted via numerical (finite element [20,21] and CUF [22-24]) approaches. In the analysis of finite amplitude vibrations of geometrically nonlinear structures the scenario is less varied, because the case study-dependent nature and computational costs of purely numerical investigations strongly limit their ability to provide fundamental insight into thermal-structural interactions via parametric studies. Thus, in this context, developing ROMs suitable for nonlinear dynamics analyses is even more important, although model reduction in coupled domains is quite challenging. Low-order models allowing the description and understanding of a number of fundamental, yet varied and intriguing, nonlinear phenomena have been used, e.g., for plates [25-29], whereas a recently proposed multimodal expansion with two generalized thermal variables and the number of mechanical ones validated through experimental investigations has been used to analyse the effects of two-way thermomechanical coupling in beam vibrations [30].

The present study is also framed within the dimension reduction issue, and aims at evaluating the reliability of a minimal thermal modelling of two-way thermomechanically coupled composite plates in view of systematic investigations of their nonlinear dynamics. Specifically, two main continuous two-dimensional (2D) models of laminated plates with von Kármán nonlinearities [31,32], recently developed within the framework of a unified formulation of the thermomechanical problem based on Tonti's approach to physical theories [33], are referred to. The two models neglect [31] or consider [32] shear deformability, and consistently assume a correspondingly linear or cubic variation of the unknown thermal field along the plate thickness. For the case of symmetric cross-ply laminates, proper and controllable dimension reduction can be accomplished for both 2D models via kinematic condensation of in-plane displacements [31,32] and shear angles [36,32] performed at the continuum and discretized level, respectively. Then, Galerkin modal reduction with a single assumed spatial dome-shape function for both mechanical and thermal variables allows to end up to minimal zero-dimensional (0D) models (with one mechanical and two thermal time-dependent equations/unknowns), which are suitable to analyse the nonlinearly coupled dynamic response in the absence of internal resonance between vibration modes. The ordinary differential equations (ODEs) of the two models are formally equal to each other, however with different coefficients and, more importantly, they still exhibit the fundamental features of geometrical nonlinearity and thermomechanical coupling embedded in the underlying, yet more complicated, continuous systems.

The simpler (shear indeformable with linear temperature) minimal model, labelled CTC (Classical Thermomechanical Coupling), has been employed for extended investigations of the plate nonlinear dynamic response under both passive [34] and active [35] thermal conditions. The former refer to a situation in which thermal phenomena are merely dragged into the structure overall response by the solely existing mechanical transverse (distributed and harmonic) excitation, as a result of the existing full coupling; the latter account for the presence of also a thermal source (of variable nature), which entails direct activation of the plate temperature field, in addition to mechanical excitation. Investigations of local and global nonlinear dynamics have highlighted the transition to mechanically- or thermally-induced buckled responses, along with the variable role played by coupling effects in different excitation conditions. In particular, active thermal excitations have shown to be of major importance not only for

originating distinct regimes of thermal response of interest in themselves, but also for meaningfully and steadily affecting the final outcome of the fast mechanical response via a non-trivial influence of the much slower transient phenomena which characterize the thermal dynamics; a behaviour unveiled via a quite refined use of topological information ensuing from global dynamics investigations [35].

Both mentioned models (shear undeformable/deformable, with correspondingly assumed linear/cubic temperature distribution) have been validated in linear free dynamics and critical buckling, versus higher-order finite element-based and analytical solutions available in the literature [32]. Yet, the major novelty of the accomplished continuum formulation and of the ensuing minimal modelling stands in complementing the assumed out-of-plane distribution of the mechanical variable with a consistent description of the transverse temperature which, depending on the assumptions' refinement, may allow us (or not) to deal with the variety of thermal excitations of possible interest in technical applications, mostly as regards the role played by thermal boundary conditions. Thus, there is a clear need to validate the thermal responses obtained by the minimal models in both transient and steady regimes with respect to those provided by reduced thermal models of higher-order and/or by analytical solutions. This will certainly affect the possibility to get a comprehensive and reliable spatio-temporal understanding of the thermal response in itself, under different thermal excitations; but it might also produce effects on the steady – and indeed much faster – mechanical response, as possibly suggested by the non-trivial role played in this respect by the slow thermal transient, as highlighted in [35] for the simplest (CTC) minimal model.

The analysis in the following aims at clarifying these points. It will be performed in view of identifying a minimal thermal modelling possibly representing the 'best' compromise among requirements of functionality, richness, flexibility and cheapness, to be variably taken into account in pursuing a systematic, yet affordable and reliable, investigation of the nonlinear dynamic response under different thermomechanical conditions, to be accomplished in a later stage.

The paper is organized as follows. The general framework for multiphysics modelling referred to for implementing a minimal, coherent and controllable, dimension reduction of the 2D continuum in view of nonlinear dynamics investigations is sketched in Sect. 2. The main features of the reference Third-order Thermomechanically Coupled (TTC) model are summarized in Sect. 3, by also comparing them with those of richer/poorer models. Section 4 is the core of the paper and presents the reconstructed spatio-temporal thermal regimes at 2D and 3D continuum levels, in terms of energy balance and temperature configuration, as resulting from an in-depth analysis of the system response under different possible combinations of thermal (boundary and body) excitations. Cross-comparisons of the outcomes of minimal models embedding variable thermal approximations are performed, along with comparisons with those provided by some analytical solutions. The main effects of thermal modelling on some aspects of the mechanical response are analysed in Sect. 5, ending up to the detection of an economical, yet overall reliable, minimal model to be used for nonlinear dynamics analyses. A conclusion section ends the paper.

2. A multiphysics modelling framework for minimal dimension reduction in nonlinear dynamics

The multiphysics modelling scheme of Fig.1 is based on Tonti diagram for physical theories [33]. It does not depend on the considered physics (symbolically indicated with 1,2, .. *N*) or on the possible space-dimensional levels (indicated with 3D, 2D, 1D, 0D) that characterize the mathematical description of the engineering problem to be tackled. That is, regardless of physics involved and dimensional level considered, it is always possible to decompose the multiphysics model (top block in Fig.1) in the three components *balance, configuration* and *phenomenology* (left, right and bottom blocks in Fig.1).

At 2D level, this scheme allowed to construct and compare different nonlinear continuous models for thermomechanical composite plate, resulting from different assumptions on the mechanical and thermal

configuration of the plate (Table 1 of [37]); by way of example, Figure 2 of [34] shows the equations and variables of the scheme (Fig.1) when particularized to the CTC model (thermomechanical plate with composite material, von Kármán geometric nonlinearities, shear indeformability, linear temperature distribution along the thickness and full thermomechanical coupling).

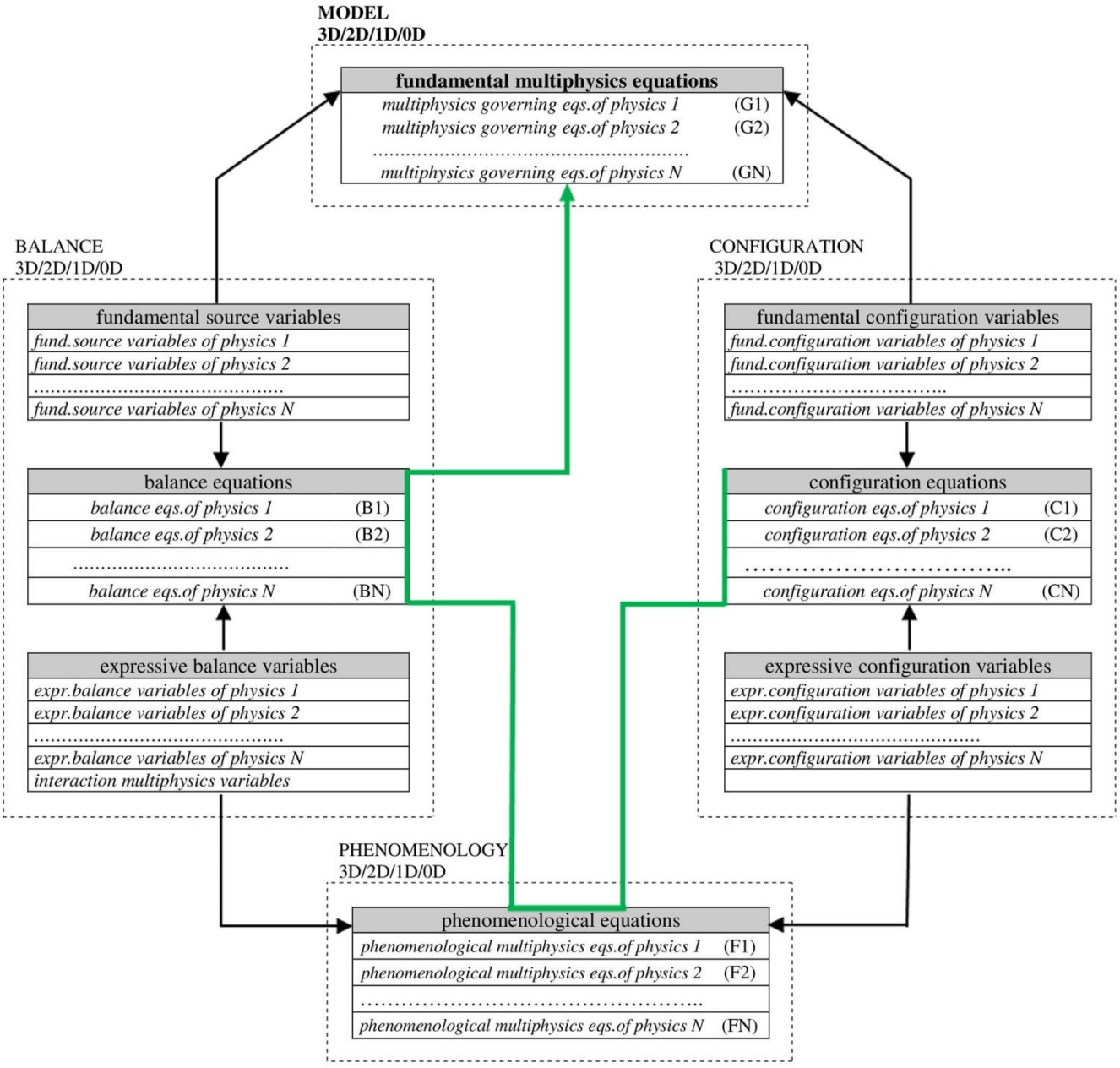

Figure 1. Unified formulation scheme for 3D / 2D / 1D / 0D multiphysics models based on Tonti diagram for physical theories.

At 0D level, starting from 2D continuous models, different nonlinear discrete models for thermomechanical composite plate were constructed and compared, resulting from different assumptions as to the greater or lower influence of various types of thermomechanical coupling (Table 2 in [37]; dynamical responses in [34], [35], [31]); as an example, in Fig.3 of [34] it is possible to see equations and variables of the scheme (Fig.1) when particularized to the CTCRa model (spatially reduced

thermomechanical plate which preserves all the two-way modelling assumptions of the underlying continuous CTC model).

The main purpose of this modelling framework is to construct, compare and select 0D *minimal* models for nonlinear dynamic analysis; for each specific nonlinear phenomenon and condition to analyse, we aim to use the model that represents the 'best' compromise among requirements of:

1) *functionality* (ability to provide reliable descriptions of the phenomenon under examination);
2) *richness* (quantity/quality of nonlinear characteristics preserved from the underlying continuous formulation, in order to allow exhaustive descriptions of the involved dynamics);
3) *flexibility* (ability to consider a variety of thermomechanical assumptions, excitations and boundary conditions of technical interest);
4) *cheapness* (ability to reduce both computational and result interpretation burden).

3. Thermal features of TTC-0D model and comparison models

We mainly consider the TTC-0D (zero-dimensional) thermomechanical model for the rectangular composite plate (Fig.2) presented in [32]. With reference to the above listed modelling requirements, the characteristics of this model are summarized in Table 1.

About model functionality, Table 1 shows that only validation in linear free dynamics (prediction of the fundamental natural frequency) and linear stability (prediction of the critical mechanical and thermal buckling) were performed [32]. In the present paper, instead, validation is carried out as regards thermal aspects, by evaluating dynamical energy balances and temperature configurations provided by the model in post-processing at the higher dimensional levels (2D and 3D) of modelling.

For all details about the TTC-0D model we refer to [32]; however, a brief summary of the main modelling features is provided.

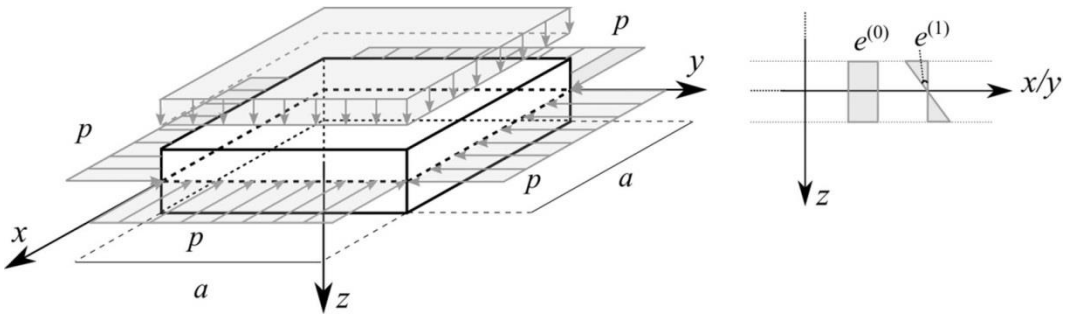

Figure 2. Laminated rectangular plate subjected to in-plane and transverse mechanical loads, and to body thermal sources distributed along the thickness.

Table 1. Characteristics of the TTC-0D model about the considered modelling requirements.

TTC-0D MODEL	
functionality	Validation in linear free dynamics and mechanical/thermal critical buckling [32].
richness	Cubic order assumption for displacement and temperature fields along the thickness, von Kármán

	nonlinearity, full thermomechanical coupling.
flexibility	- Selectable options about thermomechanical coupling: i) null coupling, ii) only membrane, iii) only bending, iv) membrane-bending, v) one-way, vi) two-way (full). - Selectable options about boundary conditions on up/down faces: i) free heat exchange, ii) thermal insulation, iii) prescribed temperature, iv) prescribed thermal flow. - Selectable options about boundary conditions on edges: i) in-plane movable edges, ii) fixed vertices, iii) prescribed temperatures. - Selectable options about excitation sources (Fig. 2): i) membrane and ii) bending mechanical load, iii) membrane and iv) bending thermal body source with linear overall distribution.
cheapness	At most 3 nonlinear ordinary differential equations

At the 3D level, the thermoelasticity coupled problem and the nonlinear Green's strain tensor simplified under the assumption of small strains and moderate rotations (von Kármán strains) are considered. As regards specifically thermal aspects, to keep the energy equilibrium we started from the following entropy balance at 3D level [38]:

$$\frac{\mathrm{d}s}{\mathrm{d}t} = -\frac{1}{T_a}\left(\mathrm{div}\mathbf{q} - E\right) \tag{1}$$

where s is the entropy, $\mathbf{q}$ is the vector of the heat flow, $T_a(x,y,z,t)$ is the absolute temperature of the plate, and E is the source energy in a unit volume and unit time. Analytical manipulations (considering the Helmholtz free energy to express the entropy in terms of temperature and strains, and inserting the Fourier law to express the heat flow in terms of temperature) and the assumption $T / T_{ref} << 1$ (where $T = T_a - T_{ref}$ is the temperature increment with respect to the reference temperature T_{ref}) allow us to obtain the following linear thermomechanically coupled heat conduction equation for the orthotropic body [38] (the lower index after the comma denotes partial differentiation)

$$\lambda_{11}T_{,xx} + \lambda_{22}T_{,yy} + \lambda_{33}T_{,zz} - \rho c_v T_{,t} - T_{ref}\left(\beta_{11}\varepsilon_{11,t} + \beta_{22}\varepsilon_{22,t}\right) + E = 0\,, \tag{2}$$

which is obtainable in [32] by inserting Eqs.(46), (47), (50), (53) and (18) into Eq.(28), and enters the top block in Fig. 1 along with the mechanical equations. In Eq.(2), the first three terms express the conductive flow (λ_{ij} are the thermal conductivities), the fourth term is relative to the internal energy (ρc_v is the thermal capacity, with ρ mass density and c_v specific heat), and the fifth term represents the thermomechanical coupling (β_{ij} are the thermoelastic coefficients and $\varepsilon_{ij,t}$ the strain rates).

At the 2D level, the basic assumptions consist of considering third-order shear deformability and von Kármán nonlinearities together with a consistently assumed cubic variation of the temperature along the plate thickness. By properly combining configuration, phenomenological and balance multiphysics relations, seven (five mechanical and two thermal) partial differential equations of motion are obtained in terms of seven unknown 2D configuration variables (Fig.1, top block) together with the corresponding boundary conditions [32].

At the 0D level, upon in-/out-of-plane static condensation and minimal Galerkin reduction, the balance equations (Fig.1, left block) of the TTC-0D model are:

$$F_{11}+F_{12}+F_{13}+F_{14}+F_{15}+F_{16}+F_{17}+F_{18}=0 \quad \text{(0D membrane-bending mechanical balance)} \tag{3a}$$

$$F_{21}+F_{22}+F_{23}+F_{24}+F_{25}+F_{26}=0 \quad \text{(0D membrane thermal balance)} \tag{3b}$$

$$F_{31}+F_{32}+F_{33}+F_{34}+F_{35}+F_{36}=0 \quad \text{(0D bending thermal balance)} \tag{3c}$$

where the quantities F_{ij} can be expressed in terms of 0D configuration variables (one mechanical and two thermal), thus obtaining three fundamental governing equations (Fig.1, top block) with structure and coefficients depending on geometric and physical characteristics of the plate, boundary conditions, and excitation sources [32].

With reference to the sole thermal balance equations (3b, c), which will be considered in the following, the balance contributions F_{ij} are linked to typical physical quantities that characterize the non-stationary thermomechanical phenomenon described by Eq.(2); these are the energy-type quantities (thermal powers) schematically shown in Table 2: *conductive flows*, *internal energy*, *thermomechanical coupling energy* and *source energy*. The table also indicates the energy contributions analogous to F_{ij} but related to the thermal balance equations at the upper 2D and 3D levels of modelling, that is equations (28) and (29) in [32] which for convenience are reported below:

$$q^{(0)}_{1,x}+q^{(0)}_{2,y}-b^{(0)}_{,t}-a^{(0)}_{,t}+Q^{(0)}+E^{(0)}=0 \quad \text{(2D membrane thermal balance)} \tag{4a}$$

$$q^{(1)}_{1,x}+q^{(1)}_{2,y}-b^{(1)}_{,t}-a^{(1)}_{,t}+Q^{(1)}+E^{(1)}=0 \quad \text{(2D bending thermal balance)} \tag{4b}$$

$$q_{1,x}+q_{2,y}+q_{3,z}-b_{,t}-a_{,t}+E=0 \quad \text{(3D thermal balance, common to all considered models)} \tag{5}$$

To construct the thermal part of the TTC-0D model, the passage from 3D level to 2D level is characterized by the following assumed cubic order polynomial shape for the 3D temperature along *z* direction (plate thickness):

$$T(x,y,z,t)=T_0+zT_1+z^2T_2+z^3T_3 \quad \rightarrow \quad T(x,y,z,t)=f_a(z)T_0+f_b(z)T_1+f_c(z)\ , \tag{6}$$

where $T(x,y,z,t)$ is the plate temperature field at 3D level (temperature increment with respect to natural state of reference), $T_0(x,y,t)$ and $T_1(x,y,t)$ are the independent temperature variables at 2D level, while $T_2(x,y,t)$ and $T_3(x,y,t)$ are quantities that can be expressed in terms of the independent variables, leading to the second expression in Eq.(6) in which $f_i(z)$ are cubic functions with coefficients depending on the considered boundary conditions [32].

Table 2. Energy contributions present in the thermal balance of TTC-0D model (Eqs. (3b, c)) and in the thermal balances at 2D (Eqs. (4)) and 3D (Eq. (5)) levels.

DESCRIPTION	0D CONTRIBUTION	2D CONTRIBUTION	3D CONTRIBUTION

contribution due to space variation along x of *conductive flow* q_1	F_{21}, F_{31}	$q_{1,x}^{(0)}$, $q_{1,x}^{(1)}$	$q_{1,x}$
contribution due to space variation along y of *conductive flow* q_2	F_{22} , F_{32}	$q_{2,y}^{(0)}$, $q_{2,y}^{(1)}$	$q_{2,y}$
contribution due to space variation along z of *conductive flow* q_3	F_{23}, F_{33}	$Q^{(0)}$, $Q^{(1)}$	$q_{3,z}$
contribution due to time variation of *internal energy* b	F_{24}, F_{34}	$b_{,t}^{(0)}$, $b_{,t}^{(1)}$	$b_{,t}$
contribution due to time variation of *coupling energy* a	F_{25} , F_{35}	$a_{,t}^{(0)}$, $a_{,t}^{(1)}$	$a_{,t}$
contribution due to *source energy* E	F_{26} , F_{36}	$E^{(0)}$, $E^{(1)}$	E

Then, we passed from 2D level to 0D level by assuming the following spatial shapes (*dome-shape*) for the 2D thermal variables along x and y directions (plate middle plane):

$$T_0(x,y,t) = T_e^m + \left(T_{R0}(t) - T_e^m\right)\sin\frac{\pi x}{a}\sin\frac{\pi y}{b} \tag{7a}$$

$$T_1(x,y,t) = T_e^b + \left(T_{R1}(t) - T_e^b\right)\sin\frac{\pi x}{a}\sin\frac{\pi y}{b} \tag{7b}$$

where $T_{R0}(t)$ and $T_{R1}(t)$ are the unknown *reduced* thermal variables (membrane and bending, respectively) of the TTC-0D model, while T_e^m and T_e^b are the components (membrane and bending) of the temperature prescribed on the plate edges.

The thermal response of the TTC-0D model just summarized will be compared with those provided by an equally cheap but less rich and flexible model (CTC-0D), and by a richer and more flexible but less cheap model (STC-0D), both referred to below.

The shear-undeformable CTC-0D model presented in [31] (to refer to for all details) is characterized by the assumption of linear distribution of the 3D temperature along z-direction (plate thickness):

$$T(x,y,z,t) = T_0 + zT_1 \tag{8}$$

(already defined symbols of Eq. (6)), and by the same assumption of TTC-0D for the 2D temperature variables (Eqs. (7)). With reference to Table 1, CTC-0D is less rich than TTC-0D as regards displacement and temperature distribution assumptions, it is less flexible because it allows to select only free heat exchange condition on the external up/down faces, and it is equally cheap because it has at most 3 balance equations formally equal to Eqs. (3) of TTC-0D (same structure, however with simpler/different expressions of the coefficients).

On the other hand, still referring to the sole thermal aspects, the STC-0D model is characterized by a polynomial seventh order shape for the 3D temperature along z direction (plate thickness):

$$T(x,y,z,t) = T_0 + zT_1 + z^2T_2 + z^3T_3 + z^4T_4 + z^5T_5 + z^6T_6 + z^7T_7 \tag{9}$$

(already defined symbols of Eq. (6)), with possibility (as in the TTC-0D model) to express two variables at 2D level in terms of the others through the boundary conditions; the assumption on the 2D independent

temperatures is similar to that of Eqs. (7) relative to TTC-0D, but contains more unknown reduced variables $T_{Ri}(t)$ because there are more variables at 2D level. With reference to Table 1 and focusing on the thermal aspect, STC-0D is considerably richer than TTC-0D about assumption on temperature distribution, it is more flexible because it allows to select also nonlinear source energy and boundary edge conditions, but it is less cheap because it has 6 energy balance equations (instead of 2 of the TTC-0D model).

When thermomechanical coupling does not significantly affect the thermal response, and for some boundary conditions, the responses of the aforementioned models will also be compared with those of two exact analytical solutions, one of non-stationary conduction and the other of stationary conduction (provided in Appendices A and B, respectively; see the electronic supplementary material, where all Appendices are reported).

4. Analysis of thermal regimes at continuum levels with energy/temperature evaluation

In the following, three different cases of thermal (boundary/body) excitation will be considered to analyse and compare thermal regimes furnished by the models in Sect.3.

Case 1 refers to a thermal boundary condition of the first kind (according to a widely used classification [40]), where all the outer surfaces of an isotropic square plate are instantaneously heated to the same temperature. TTC-0D and STC-0D model are compared with each other, and with a non-stationary conduction analytical solution [40] assumed as reference (Appendix A). The outcome of the most refined STC-0D model is seen to be closer to the analytical solution than the TTC-0D outcome, and STC-0D is thus assumed as reference in the other two cases.

Case 2 refers to a mixed thermal boundary condition of second and first kind [40], where prescribed thermal flow and temperature are imposed on the up and down outer surfaces, respectively, of a thermally orthotropic square plate. A stationary conduction analytical solution [39] (Appendix B) is used to verify the response of the models after the non-stationary conduction phase.

Case 3 refers to a thermal boundary condition of third kind [40] with additional body source, where a free heat exchange is allowed on the up/down outer surfaces of a thermally orthotropic square plate, while a source energy acts inside the plate. Free heat exchange is the sole boundary condition to be possibly prescribed on the up/down faces with the simpler CTC-0D model, whose outcomes are also considered in the comparisons. This model, in fact, is strongly limited by the assumption of linear distribution of the 3D temperature (Eq.(8)); indeed, for example, if a prescribed temperature were imposed on the outer surfaces, it would be instantaneously accommodated by the linear distribution on the thickness, and no thermal dynamics would be possible; similar considerations can be made when a prescribed thermal flow is assigned, a case in which the dynamics would be excessively constrained [31].

Although the present modelling framework accounts for two-way (from mechanical to thermal, and from thermal to mechanical) coupling, we neglect the mechanical coupling terms in the thermal equations of the models (terms F_{25}, F_{35} in Eqs.(3b,c)), for the sake of simplicity. In fact, when an active thermal regime is considered, their effects in the thermal equations are negligible with respect to the direct ones of the applied thermal loads [41].

4.1 Case 1: Temperature prescribed on the up/down faces and edge faces

We consider an isotropic square plate of side $a = 1\,\mathrm{m}$, thickness $h = 0.05\,\mathrm{m}$, and material AL2024 with mass density $\rho = 2800$ kg/m^3 and the following thermal properties [32]: specific heat at constant strain

$c_v = 897$ J/(kg·K), thermal conductivities along the *x*, *y* and *z* axes $\lambda_{11} = \lambda_{22} = \lambda_{33} = 130$ W/(m·K), thermal expansions along *x* and *y* $\alpha_1 = \alpha_2 = 25 \times 10^{-6}$ 1/K.

At the initial time instant all the 6 external faces of the plate are instantaneously heated to the same temperature, which is then maintained constant. To reproduce this condition in the present modelling framework, we impose on the up/down faces:

$$T\big|_{z=\pm h/2} = T^*, \tag{10}$$

where the first member expresses the plate temperature $T(x, y, z, t)$ at the lowest and highest levels, while the second member expresses the prescribed temperature T^* on the outer faces. We impose the same spatially constant temperature T^* also on the edge faces, by setting into Eqs. (7):

$$T_e^m = T^*, \quad T_e^b = 0 \tag{11}$$

For these boundary conditions, thermal balance equations (3b,c) of the TTC-0D model in terms of unknowns $T_{R0}(t)$ and $T_{R1}(t)$ (membrane and bending temperatures) read [32] (Fig.1, top block):

$$a_{21}\dot{T}_{R0} + a_{22}T_{R0} + 2a_{23}T^* + a_{25}e^{(0)}(t) = 0 \tag{12a}$$

$$a_{31}\dot{T}_{R1} + a_{32}T_{R1} + a_{34}e^{(1)}(t) = 0 \tag{12b}$$

where the dot denotes time derivative, $e^{(0)}(t)$ and $e^{(1)}(t)$ represent thermal excitation sources (see Sect. 4.3 forward), and expressions of coefficients a_{ij} are reported in Appendix C; note the non-sequential coefficients numbering due to the neglected mechanical coupling terms. The corresponding equations for the STC-0D model are reported in Appendix D.

Setting $T^* = 100$ K and body source energy equal to zero, Eqs.(12) provide the thermal dynamics shown in Fig. 3: since imposed conditions are symmetrical, the bending component $T_{R1}(t)$ is not activated.

The relative energy contributions to the membrane thermal balance (Eq.(3b)) is shown in Fig. 4a together with their sum, which at 0D level is always zero for obvious mathematical reasons. Remembering physical quantities which each of these contributions is linked to (Table 2), we can

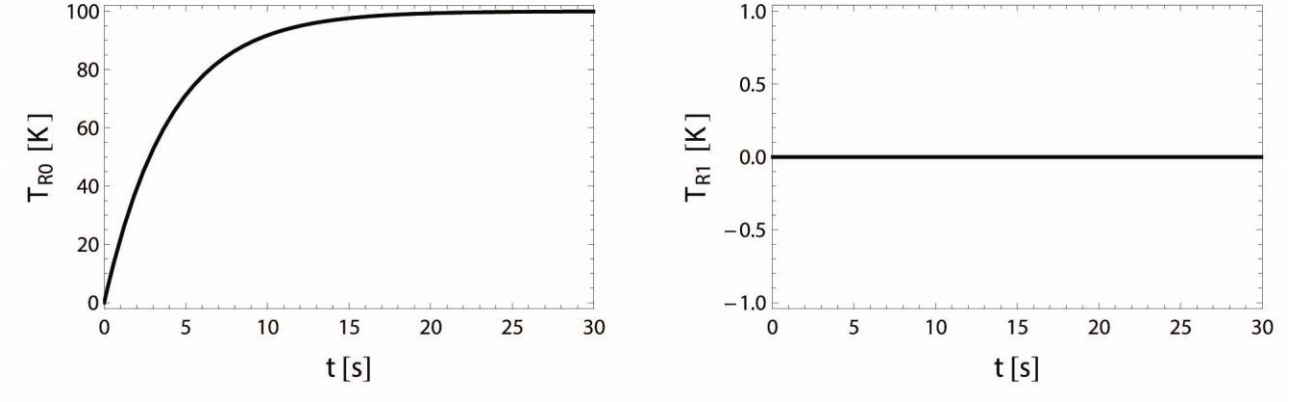

Figure 3. Case 1, time history of the thermal variables of TTC-0D model.

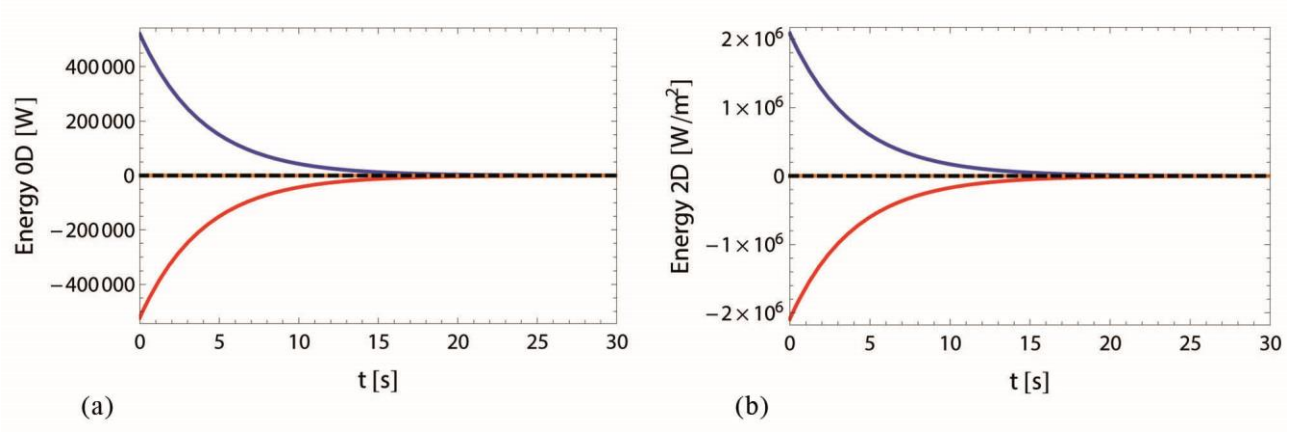

Figure 4. Time history of energy contributions to the membrane thermal balance at 0D (a) and 2D (b) levels, and of their sum, for the TTC-0D model. Colours (on-line): contributions due to internal energy (red) and to conductive flow along *z* (blue), *y* (green), and *x* (magenta), and their sum (black dashed)

recognize the essential characteristics of the thermal phenomenon under examination already at 0D level (Fig. 4a): the temperature prescribed on all the outer faces activates a non-stationary conduction where the increase of internal energy (red) balances the decrease of conductive flows (blue, green, magenta) at each time instant, until thermal equilibrium is reached (when all internal points of the plate have reached the temperature of 100 K prescribed on the external faces). The contributions related to conductive flows along *x* and *y* directions (green and magenta) are not perceptible in Fig. 4a because they are very small compared to the flow contribution along *z* (blue), due to the small plate thickness considered.

Analogously to Fig. 4a, Figure 4b shows the energy contributions to the 2D membrane balance (Table 2, Eq. (4a)) for the point in the centre of plate mid-plane, and is obtained in post-processing from the time history of the 0D model variable $T_{R0}(t)$ (TTC-0D). We can see (Fig. 4b, dashed black line) that the 2D balance is satisfied at all times; this also happens at all points of the plate mid-plane, as confirmed by the exact closed form solution obtained for Eq. (4a) expressed in terms of temperature, particularized for this case and without thermomechanical coupling and source contributions (Appendix E).

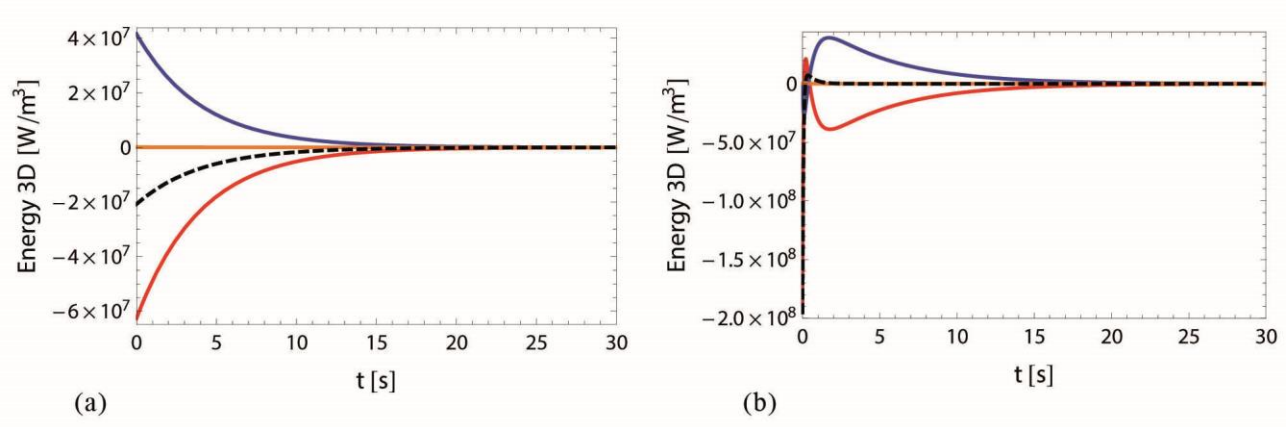

Figure 5. Time history of energy contributions to thermal balance 3D, and of their sum, in the centre of solid ($x = a/2,\ y = b/2,\ z = 0$), associated with TTC-0D (a) and STC-0D (b) model. Colours (on-line): contributions due to internal energy (red), and to flow along *z* (blue), *y* (green), and *x* (magenta), and their sum (black dashed)

Figure 5a shows the energy contributions to the 3D balance (Table 2, Eq. (5)) for the point in the centre of the solid (always obtained in post-processing, starting from the response of the 0D model). Contrary to the 2D level (Fig. 4b), in the 3D balance the time-varying contributions due to internal energy and conductive flow along z are not symmetrical with each other, thus producing an energetic imbalance (dashed black line) which is also present with a variable degree in all points of the solid. It depends on the 3D temperature configuration $T(x, y, z, t)$ ensuing from the assumed modelling (Eqs. (6) and (7)), whose mathematical characteristics (derivatives at every point and instant) differ from those of the analytically exact solution of the 3D problem. In fact, the 3D balance of Eq. (5) in terms of temperature (neglecting coupling terms) is expressed by the heat equation:

$$\lambda_{11} T_{,xx} + \lambda_{22} T_{,yy} + \lambda_{33} T_{,zz} - \rho c_v T_{,t} = 0 , \tag{13}$$

where curvature terms of the temperature function with respect to space (second derivatives $\lambda_{ii} T_{,jj}$, due to conductive flow) should be balanced by the tangent line term with respect to time (first derivative $\rho c_v T_{,t}$, due to internal energy).

Figure 5b shows the 3D balance for the model STC-0D, analogous to Fig. 5a. The energetic imbalance (dashed black line) reaches its minimum value much faster than for the TTC-0D model (Fig. 5a), due to a diagram of single contributions that is globally more symmetrical than that in Fig. 5a. Actually, it can be noted that at the initial instant and in the first few hundredths of second, a marked energetic imbalance occurs for STC-0D (Fig. 5b), higher than the TTC-0D one. This is because at $t = 0\ s$ the internal energy contribution (red line in Fig. 5b and term $\rho c_v T_{,t}$ in Eq.13) is very large, while the conductive flow contribution (blue line in Fig. 5b and term $\lambda_{33} T_{,zz}$ in Eq.13) is zero; thus, in these initial instants, the seventh-order shape assumed for the temperature in the formulation of STC-0D model (Eq. (9)) loosely satisfies the heat equation (13).

However, in general, the energetic imbalance of the models at certain points and instants provides no direct hints as to how much the thermal response is close to (or away from) the real one. Thus, to evaluate the response provided in this case by the two models, in the following we assume as reference the non-stationary analytical solution in convergent series reported in Appendix A.

The above shown 3D energy imbalances of TTC-0D and STC-0D are superimposed in Fig. 6b and the corresponding 3D temperature curves are shown in Fig. 6a, by also reporting the graphs provided by the non-stationary analytical solution with 5 or 20 terms in the series. The temperature curve of STC-0D (blue) agrees well with that provided by the 20-term analytical solution (gray), which is here assumed as benchmark. The temperature curve of the 5-term analytical solution (green) provides a bad estimate at the first seconds of conduction, because it starts from a high and unrealistic negative temperature value, but then it approaches the curves of greater precision. The temperature curve of TTC-0D model (red) correctly presents a zero temperature value at the initial instant and grows without inflection points, however overestimating the transient temperature.

The balance aspects are checked in more detail in Fig. 6c,d, by comparing the single energy-type contributions to the 3D balance of the two models with those deduced from the analytical solution. For the STC-0D model, both the internal energy contribution b and the conductive flow contribution q_3 along z are very close to the reference quantities; instead, the TTC-0D model shows greater deviations.

Figure 7 shows the temperature curves along the thickness, at the instants $t = 0\ \mathrm{s}$, $t = 0.3\ \mathrm{s}$, $t = 10\ \mathrm{s}$ and $t = 30\ \mathrm{s}$, respectively. Remembering the boundary conditions of this case, at $t = 0$ the real temperature is zero along the whole thickness except at the extreme levels (where it is $T = 100\mathrm{K}$); therefore, neither TTC-0D nor STC-0D allow to describe well the real temperature at the initial instant (Fig. 7a). Compared to TTC-0D, STC-0D produces a better profile due to the seventh-order assumption in

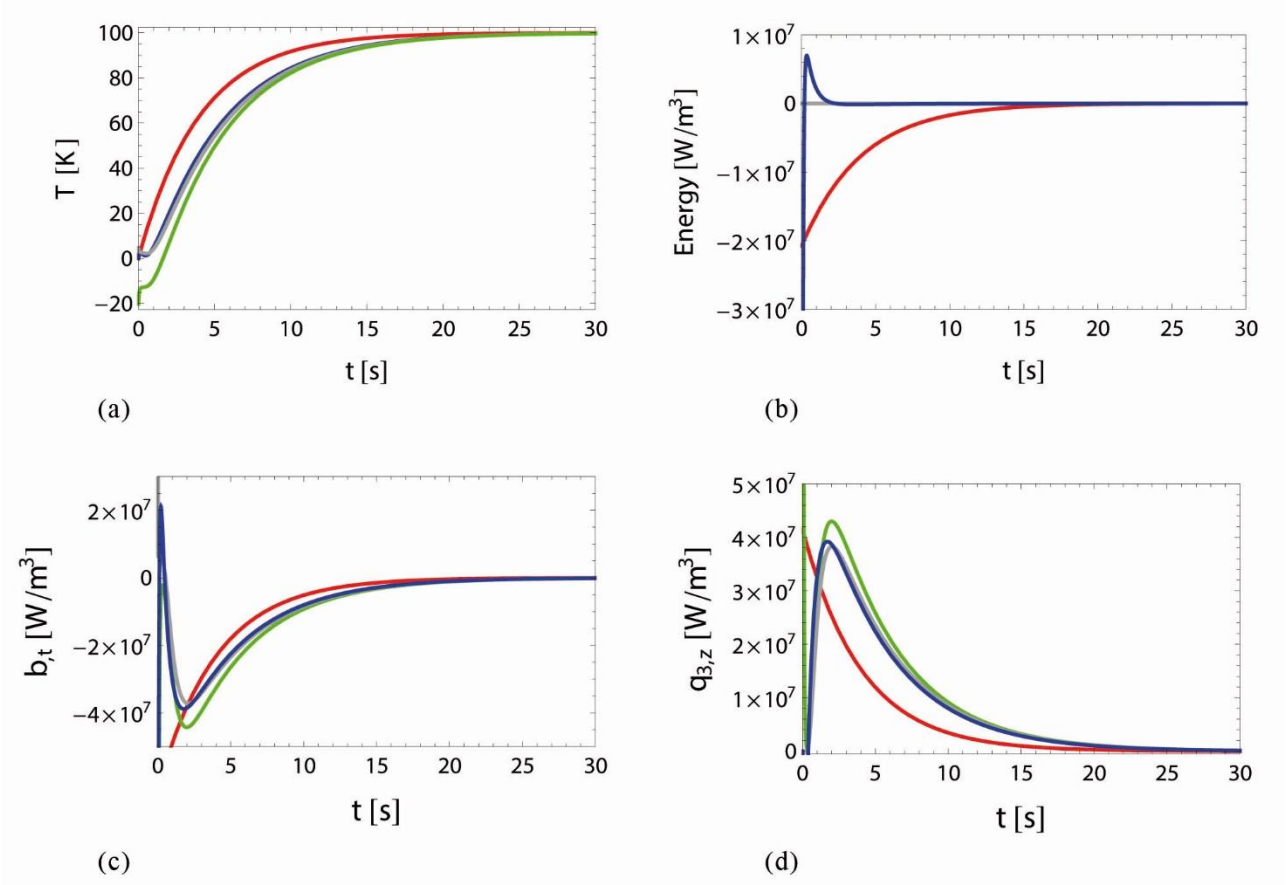

Figure 6. Time history of 3D temperature (a), energy contributions sum (b), single contributions due to internal energy (c) and to conductive flow in *z* direction (d), in the centre of solid ($x = a/2$, $y = b/2$, $z = 0$), for TTC-0D (red) and STC-0D (blue) models, and with the 5-term (green) and 20-term (gray) analytical solutions. (Colours on-line)

Eq.(9) but, if a better descriptive capacity were required, it would be necessary to consider a model with a higher temperature order.

Compared to TTC-0D, STC-0D produces a better profile due to the seventh-order assumption in Eq.(9) but, if a better descriptive capacity were required, it would be necessary to consider a model with a higher temperature order. However, just after the initial instant, the temperature profile of the STC-0D model remains (for the whole time evolution) very close to that of the 20-term analytical solution; instead, the TTC-0D model shows a general overestimation of the temperature (Fig. 7b,c). As regards energy balance aspects along the thickness (graphs not reported for the sake of brevity), the shapes of the STC-0D contributions due to both the internal energy b and the conductive flow q_3 along *z* are overall more similar (and closer) to the reference quantities than the corresponding ones of TTC-0D; this does not occur for the quasi-stationary ($t = 30$ s) q_3 flow of STC-0D, which is considerably away from the reference one, although the temperature equal to 100 K is correctly provided (Fig.7d). This is due to the seventh-order shape assumed for the temperature of STC, that globally improves the thermal response (with respect to TTC) but introduces residual numerical balance errors at the end of the dynamics.

Figure 8 shows the temperature graphs plotted along *x* direction, at mid-plane level and *y* half-size. Remembering again the boundary conditions, at $t = 0$ s the real temperature is zero along the whole *x* direction except on the edges (where it is $T = 100$ K); therefore in Fig. 8a, unlike Fig.7a related to the

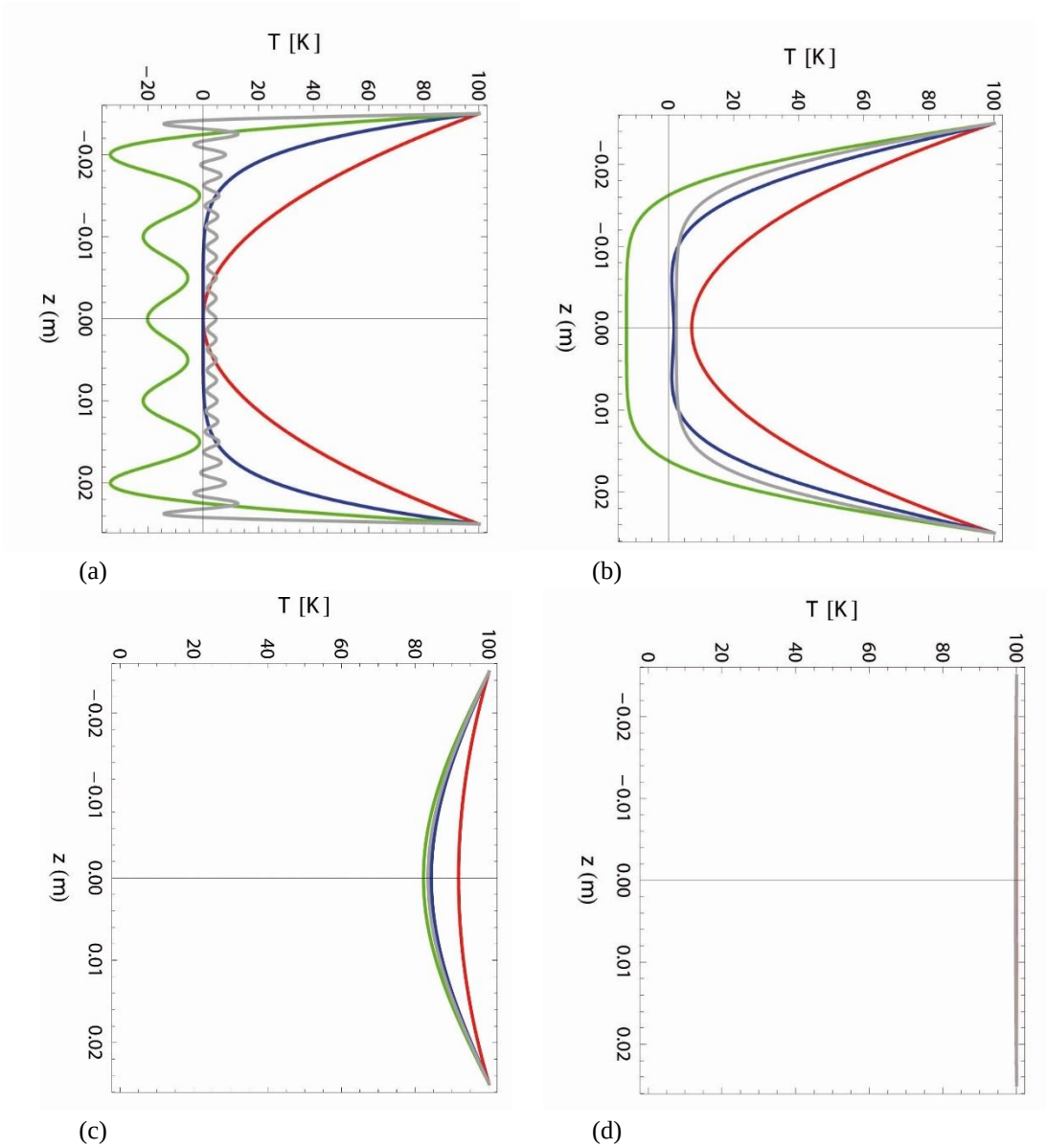

Figure 7. Temperature profiles along z (thickness) direction, in the central point ($x = a/2$, $y = b/2$), at instants: $t = 0$ s (a), $t = 0.3$ s (b), $t = 10$ s (c), $t = 30$ s (d), . Colours (on-line): TTC-0D (red) and STC-0D (blue) models, 5-term (green) and 20-term (gray) analytical solutions.

temperature profile along the thickness, STC-0D (although providing the correct temperature in the centre) implies the same shape error of TTC-0D, which still persists (Fig.8c) until about the steady conditions ($t = 30$ s, Fig. 8d). This is due to the different mathematical assumption of the prescribed constant temperature on the boundary with respect to the assumed internal 2D dome-shape temperatures. To improve the approximation, a multimodal thermal shape along x and y could be considered instead of the single-mode one (see Eq.7 related to TTC), but this would result in an increase of the number of equations. Based on the analyses carried out, a few summary points can be made.

(i) In the centre of the plate/solid, the most refined STC-0D model is very close to the 20-term analytical solution (for the whole time evolution). Instead, the TTC-0D model (slightly) overestimates the temperature during the transient.

(ii) Such response features of the two models also hold in the centre along the whole thickness, with STC better approaching the expected physical temperature distribution also in the very first initial instants.

(iii) Along the *x* direction, at mid-plane level and *y* half-size, STC-0D implies almost the same shape error of TTC-0D during the transient, due to the different assumptions for the 2D internal and the boundary prescribed temperatures.

Based on these results, in the following two cases the model STC-0D will be assumed as reference to compare cheaper models as TTC-0D and CTC-0D. However, to eliminate the error shape along the direction of plate edges (point (iii)), the same dome-shape spatial distribution of thermal loads as of the 2D internal temperatures will be assumed.

4.2 Case 2: Flow and temperature prescribed on the up/down faces

We consider a square single-layer epoxy/carbon fibre composite orthotropic plate of side $a = 1\,\mathrm{m}$, thickness $h = 0.1\,\mathrm{m}$, with mass density $\rho = 1940$ kg/m^3 and thermal properties [35]: specific heat at constant strain $c_v = 400$ J/(kg·K), thermal conductivities along *x*, *y* and *z* $\lambda_{11} = 36.42$, $\lambda_{22} = \lambda_{33} = 0.96$ W/(m·K), thermal expansions along *x* and *y* $\alpha_1 = 0.57\times10^{-6}$, $\alpha_2 = 35.6\times10^{-6}$ 1/K, boundary conductance $H = 100$ W/(m^2·K).

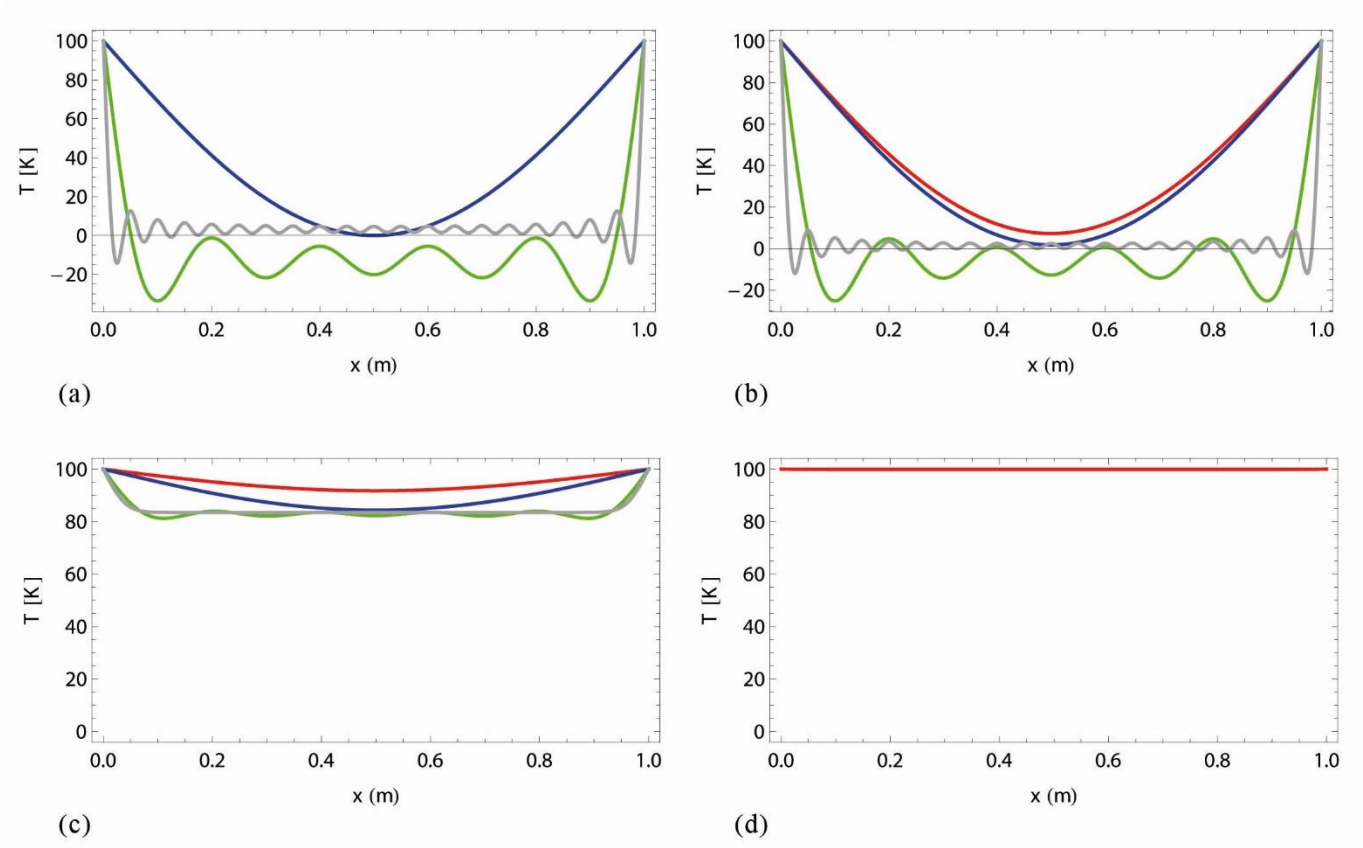

Figure 8. Temperature profiles along *x* direction, at points $y = b/2$, $z = 0$, at instants $t = 0$ s (a), $t = 0.3$ s (b), $t = 10$ s (c), $t = 30$ s (d) . Colours (on-line): TTC-0D (red) and STC-0D (blue) models, 5-term (green) and 20-term (gray) analytical solutions.

At the initial instant an irradiation thermal flow acts on the upper face, while the lower face is instantaneously heated to a given temperature; both thermal loads are considered constant during the whole thermal process. At the edges, temperature variations are prevented (cold edges).

To reproduce this condition, we impose on the faces:

$$q_3\big|_{z=-h/2} = q^* \sin\frac{\pi x}{a}\sin\frac{\pi y}{b} \tag{14a}$$

$$T\big|_{z=h/2} = T^* \sin\frac{\pi x}{a}\sin\frac{\pi y}{b} \tag{14b}$$

where the l.h.s. express the conductive flow $q_3(x,y,z,t)$ (z-direction) and the plate temperature $T(x,y,z,t)$ at the extreme levels, respectively, while the r.h.s. express the prescribed flow and temperature (with amplitudes q^* and T^*) on the outer faces; we assume that both these thermal loads have a trigonometric spatial shape, coinciding with the one assumed for the internal distribution of 2D temperatures (dome-shaped, Eq. (7)). To impose a zero temperature variation on the edges (cold edges), let us put $T_e^m = T_e^b = 0$ in Eq. (7).

For these boundary conditions, thermal balance equations (3b,c) of the TTC-0D model in terms of unknowns $T_{R0}(t)$ and $T_{R1}(t)$ (membrane and bending temperatures) read [32]:

$$a_{21}\dot{T}_{R0} + a_{22}T_{R0} + a_{23}\dot{T}_{R1} + a_{24}T_{R1} + a_{25}q^* + a_{26}T^* + a_{28}e^{(0)}(t) = 0 \tag{15a}$$

$$a_{31}\dot{T}_{R0} + a_{32}T_{R0} + a_{33}\dot{T}_{R1} + a_{34}T_{R1} + a_{35}q^* + a_{36}T^* + a_{38}e^{(1)}(t) = 0 \tag{15b}$$

with $e^{(0)}(t)$ and $e^{(1)}(t)$ thermal excitation sources, and coefficients a_{ij} given in Appendix C. The corresponding equations for the STC model are reported in Appendix D.

Setting $q^* = 2\times10^3$ W/m^2, $T^* = 10$ K and body source energy equal to zero, Eqs.(15) provide the thermal dynamics shown in Fig.9 . Contrary to previous Case 1, here also the bending component $T_{R1}(t)$ is activated, since the thermal loads on the upper and lower faces are not symmetrical. Moreover, the different nature of the two thermal boundary conditions of this mixed case implies a coupling between equations (15), whose equal structure entails that the variables $T_{R0}(t)$ and $T_{R1}(t)$ reach the stationary phase at the same time (considerably longer than that of Case 1 for physical reasons).

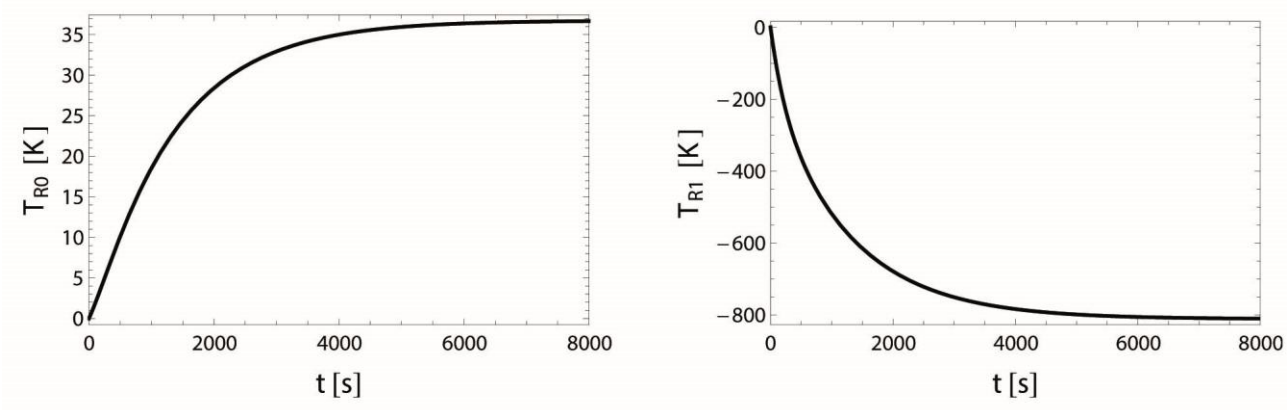

Figure 9. Case 2, time history of the thermal variables of TTC-0D model.

The graphs of the relative 2D energy contributions (obtained in post-processing from the TTC-0D model response and not reported) show that the 2D membrane and bending balances are satisfied at all times and all points of plate mid-plane, as confirmed by the exact closed form solution obtained for Eqs.(4a, b) (expressed in terms of temperatures) and reported in Appendix F for the present case.

Figure 10a shows instead the corresponding graphs of the 3D energy balance contributions (Table 2, Eq. (5)) in the central point of the solid (always obtained in post-processing). With respect to the isotropic plate of Case 1, the flows along *x* and *y* furnish different contributions, due to the marked difference of the corresponding thermal conductivities for the orthotropic plate considered herein. The energetic imbalance (dashed black line) strongly decreases as the conduction stationary state is approached, up to stabilizing onto a value of about $2576\ \mathrm{W/m^3}$. To evaluate the modelling error provided in this case by the TTC-0D model, some comparisons are made.

The imbalance of STC-0D is also shown in Fig.10a (dashed blue line); it reaches its barely detectable minimum value (about $0.38\ \mathrm{W/m^3}$) much faster than TTC-0D does with its minimum. Figure 10b shows the corresponding 3D temperatures, where the curves of the two models are seen to be very close, with steady values of about 36.4 K (TTC-0D) and 37.3 K (STC-0D). Like Case 1, the STC-0D model involves a marked energetic imbalance at the very beginning of the dynamics (Fig. 10a), which however does not significantly affect the temperature values.

Figure 11 shows the temperature predictions provided by the two models in the central point of the plate along the thickness, at $t = 0\ s$, $t = 200\ s$ and $t = 8000\ s$. The quite dissimilar temperatures initially provided by the two models (mostly at the upper points far away from the mid-plane) still persist at $t = 200\ \mathrm{s}$ (Fig. 11b); however, when the stationary state is reached, the corresponding temperature curves are almost coincident, with the STC-0D one perfectly coinciding with the curve (gray, but not visible) of the exact stationary analytical solution (Appendix B).

As regards the energy balance aspect along thickness (graphs not reported), at stationary state ($t = 8000\ \mathrm{s}$) the STC-0D model is well balanced while the TTC model shows an imbalance. It can be mathematically explained by remembering the cubic assumption of temperature 3D (Eq.(6)) and observing the consequent curves of the single contributions $b_{,t}$, $q_{3.z}$, $q_{2.y}$, $q_{1.x}$ to the 3D balance (Eq.(5), Table 2), not

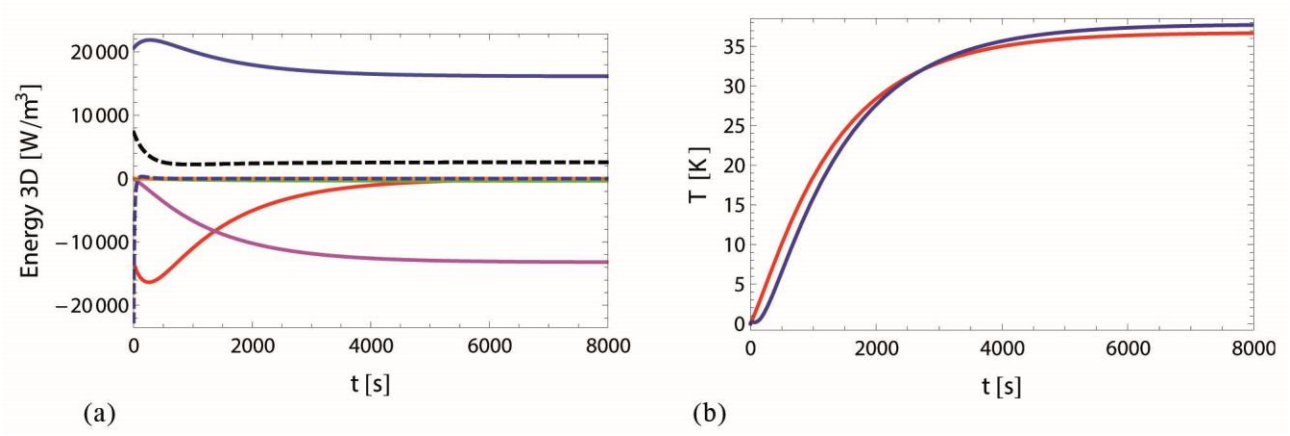

Figure 10. Time history of energy contributions to 3D thermal balance, and of their sum, for the TTC-0D model, and sum of energy contributions, for the STC-0D model (a); 3D temperatures for TTC-0D and STC-0D models (b); all in the centre of solid ($x = a/2,\ y = b/2,\ z = 0$). Colours (on-line): TTC-0D contributions due to internal energy (red), to flow along *z* (blue), *y* (green), and *x* (magenta), and sum of contributions (black dashed); STC-0D sum of contributions (blue dashed) (a); TTC-0D (red) and STC-0D (blue) temperatures (b).

shown for the sake of brevity. While the internal energy contribution $b_{,t}$ correctly vanishes, the flow contribution $q_{3.z}$, which is a linear curve ($q_{3,z} = \lambda_{33} T_{,zz}$), is unable to balance along the thickness the flow contribution $q_{1,x}$, which is a nonlinear curve ($q_{1,x} = \lambda_{11} T_{,xx}$) (the contribution $q_{2,y}$ is small compared to $q_{1,x}$ because the material is strongly thermally orthotropic). Instead, the STC model does not show imbalance because also the contribution $q_{3.z}$ is a nonlinear curve (remind the temperature assumption of Eq.(9)), which is able to balance the nonlinear contribution $q_{1.x}$ along the thickness.

Graphs along *x* and *y* directions (like Fig. 8 of Case 1) are not shown; in fact, they do not exhibit any shape error as regards temperature distribution, because the flow and temperature prescribed on the external faces in the present case have been given the same dome-shape as for the 2D internal temperatures (compare Eqs. (14) and (7)). Instead, in the case of different spatial distributions of thermal loads on the faces, an error would occur due to the coarse monomodal assumption of the internal temperatures.

4.3 Case 3: Free heat exchange on the up/down faces and active source energy

We consider a square single-layer orthotropic plate of side $a = 1\,\mathrm{m}$, with the same properties of case 2. A free convective exchange with the surrounding medium is allowed on the up/down outer faces. At the initial instant a body source energy acts inside the plate (due, e.g., to the passage of electric current), with intensity varying proportionally along the thickness between two assigned extreme values. This thermal load is maintained constant during the whole process. At the edges, temperature variations are prevented (cold edges).

To reproduce the condition on the faces, we impose:

$$q_3\big|_{z=\pm h/2} = \pm H\left[T_\infty - (T)_{\pm h/2}\right] \tag{16}$$

where the l.h.s. expresses the conductive flow $q_3(x, y, z, t)$ (*z*-direction) at the up/down levels of the plate, while the r.h.s. expresses Newton's law of cooling, with H convection coefficient and T_∞ constant temperature difference between the absolute temperature of surrounding medium and the reference one. Note that this is the sole boundary condition on the external faces to be possibly prescribed with the

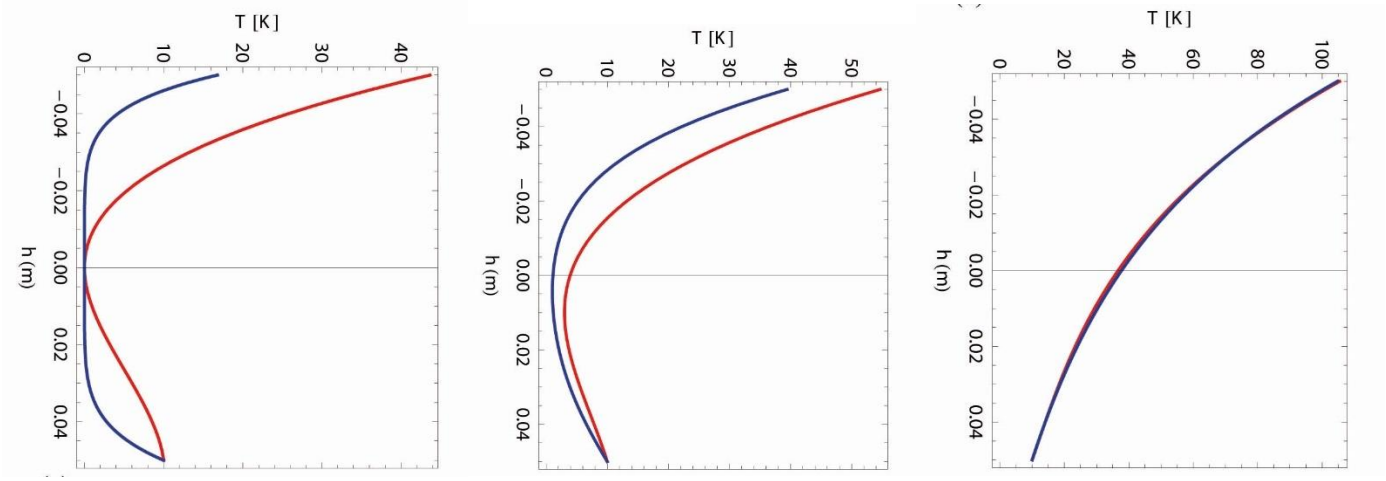

(a) (b) (c)

Figure 11. Temperature profiles, along *z* (thickness) direction, in the central points ($x = a/2$, $y = b/2$), at instants $t = 0$ s (a), $t = 200$ s (b), and $t = 8000$ s (c). Colours (on-line): TTC-0D (red) and STC-0D (blue) models, exact stationary analytical solution in Appendix B (grey).

simpler CTC model (based on a linear distribution of 3D temperature along the thickness, Eq. (6)), whose outcomes will be then considered in the following comparisons, too. To impose a zero temperature variation on the edges, let us put $T_e^m = T_e^b = 0$ in Eq. (7).

To consider the thermal load distribution linearly varying along the thickness, the following law for the body source energy *E* (Fig.12) is assumed in the 3D balance (Eq. (5), Table 2):

$$E(x,y,z,t) = E^C(x,y,t) + z\ E^L(x,y,t) \tag{17}$$

where a trigonometric shape is given to the membrane $E^C(x,y,t)$ and bending $E^L(x,y,t)$ sources (the same dome-shape as that of 2D temperature variables in Eq.(7)):

$$E^C(x,y,t) = e^{(0)}(t)\sin\frac{\pi x}{a}\sin\frac{\pi y}{b} \tag{18a}$$

$$E^L(x,y,t) = e^{(1)}(t)\sin\frac{\pi x}{a}\sin\frac{\pi y}{b} \tag{18b}$$

The source energies $E^{(0)}(x,y,t)$ and $E^{(1)}(x,y,t)$ of 2D balance (Eqs. (4), Table 2) are linked to the 3D source energy *E* of Eq.(17) by the relationship [32,35]:

$$E^{(0)} = \int_{-h/2}^{h/2} E dz\ ,\quad E^{(1)} = \int_{-h/2}^{h/2} zE dz; \tag{19}$$

For these boundary conditions, thermal balance equations (3b,c) of the TTC-0D model in terms of unknowns $T_{R0}(t)$ and $T_{R1}(t)$ (membrane and bending temperatures) are [32]:

$$a_{21}\dot{T}_{R0} + a_{22}T_{R0} + a_{23}T_\infty + a_{25}e^{(0)}(t) = 0 \tag{20a}$$

$$a_{31}\dot{T}_{R1} + a_{32}T_{R1} + a_{34}e^{(1)}(t) = 0 \tag{20b}$$

with $e^{(0)}(t)$ and $e^{(1)}(t)$ thermal excitation sources, and coefficients a_{ij} given in Appendix C. The corresponding equations for the STC model are reported in Appendix D, while those of the CTC model have the same structure of the TTC ones (with different coefficients).

Setting $e^{(0)} = 2\times10^4$ W/m^3 and $e^{(1)} = 2\times10^6$ W/m^4, $h = 0.1$ m, $T_\infty = 0$, Eqs.(20) provide the thermal dynamics shown in Fig.13.

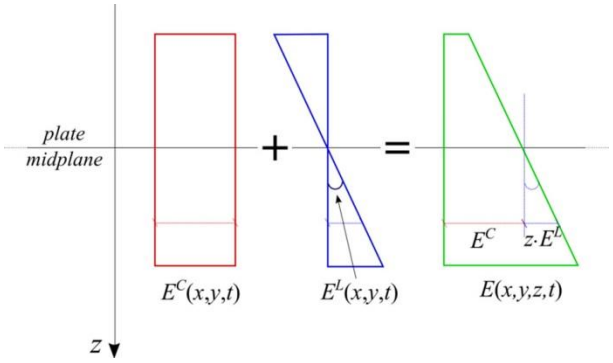

Figure 12. Contributions to the body source energy distribution along the plate thickness.

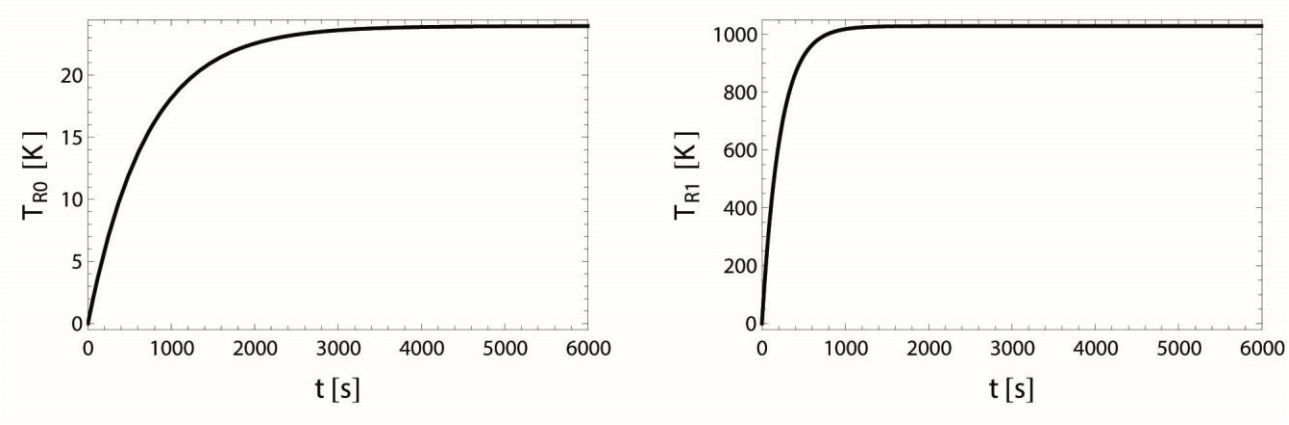

Figure 13. Time history of the thermal variables of TTC-0D model.

Contrary to the previous Case 2, the equal boundary conditions prescribed on the upper and lower faces imply decoupling of the two equations (20), with the independent dynamics of the two variables having speeds (quite different from each other for physical reasons) governed by the coefficients a_{21} and a_{31}.

The graphs of the relative 2D energy contributions (not reported) show that the 2D membrane and bending balances are satisfied at all times and all points of plate mid-plane, as confirmed by the exact closed form solution obtained for Eqs.(4a,b) (expressed in terms of temperatures) and reported in Appendix G for the present case.

Figure 14a compares the 3D temperature curves provided by TTC-0D with those of STC-0D and CTC-0D models, in the central point of the solid, while Figure 14b shows the corresponding energy imbalances. The CTC-0D model exhibits the highest energy imbalance and a temperature curve very far from those of the other two models (with a stationary value significantly lower); instead, the temperature curves of TTC-0D and STC-0D are quite close to each other.

Figure 15 shows the temperature predictions provided by the three models in the central point of the plate along the whole thickness, at $t = 0\ s$, $t = 100\ s$ and $t = 6000\ s$. All models exhibit a more marked temperature increase in the lower part of the plate, due to the considered power density distribution along the thickness (Fig. 12); however, the maxima of the more refined models are not located at the up/down surfaces, possibly due to heat dissipation towards the environment occurring therein.

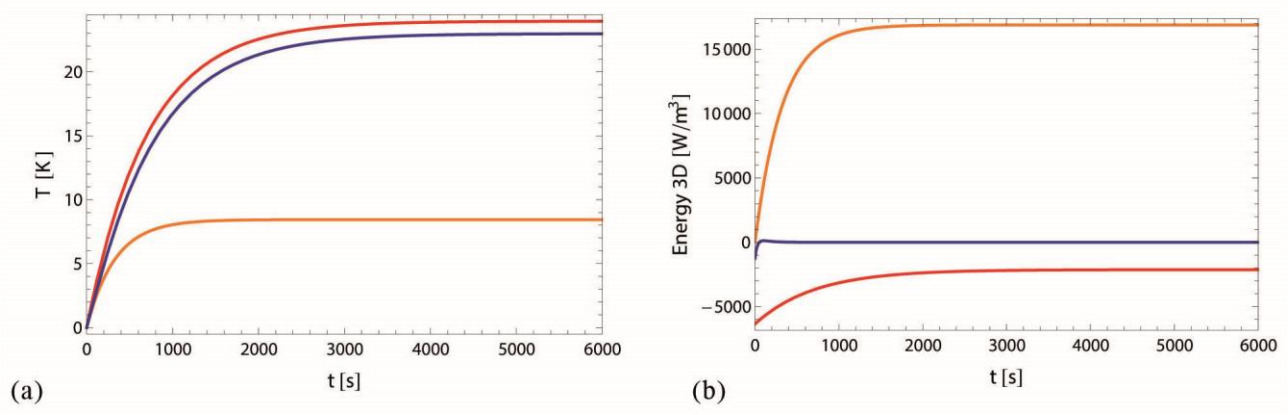

Figure 14. Time history of 3D temperature (a) and energy contributions sum (b), in the centre of solid ($x = a/2,\ y = b/2,\ z = 0$), $h = 0.1$ m, for TTC-0D (red), STC-0D (blue) and CTC-0D (orange) models. (Colours on-line).

In the stationary phase ($t = 6000\ s$, Fig. 15c), the temperature profile of CTC-0D exhibits a considerable deviation from those of TTC-0D and STC-0D, which are instead very close to each other and practically coincide in many zones. Obviously, the CTC-0D model is much penalized by its linear temperature distribution assumption (Eq. (8)), which entails analytical vanishing of the q_3 thermal flow contribution to the 3D balance; however, the overall effect of such a flow along the thickness is considered in the 2D balance through the contributions $Q^{(0)}$ and $Q^{(1)}$ in Eqs.(4b,c) and Table 2 [31]. As regards balance aspects along the whole thickness (not reported), the STC-0D model is globally more balanced, while the CTC-0D model exhibits the highest imbalance.

Again, graphs along *x* and *y* directions are omitted, since they do not show any shape error of the temperature distribution; this is because the source energy acting inside the plate has been given the same dome-shape as the 2D temperature variables (compare Eqs. (18) and (7)). In the case of other spatial distributions of thermal loads inside the plate, differences would arise.

Finally, we consider a plate that differs from the previous one only for a smaller thickness, equal to $h = 0.01\ \mathrm{m}$ (results not shown). If maintaining the same source energy, the duration of all transient is much shorter, as expected, and temperature curves of TTC-0D and STC-0D practically coincide both in the central point and along the thickness. Of course, the temperature curve of CTC-0D is closer to those of the other two models than in the thick plate.

Instead, if greater intensities of the source energy are considered (e.g., $e^{(0)} = 8\times10^{5}\ \mathrm{W/m^3}$ and $e^{(1)} = 1.15\times10^{9}\ \mathrm{W/m^4}$, also used in the following section), CTC-0D shows considerable differences compared to TTC-0D and STC-0D, despite the very small thickness. As regards temperature profile, although attaining practically equal values at the extreme surfaces, the CTC one considerable deviates from the others also in the stationary phase, notwithstanding possible expectations about the ability of the assumed linear temperature distribution to accurately describe one-dimensional steady-state heat conduction (see, e.g., [30] for a beam).

For this latter case, a comparison of also mechanical aspects of the response will be performed in the next section.

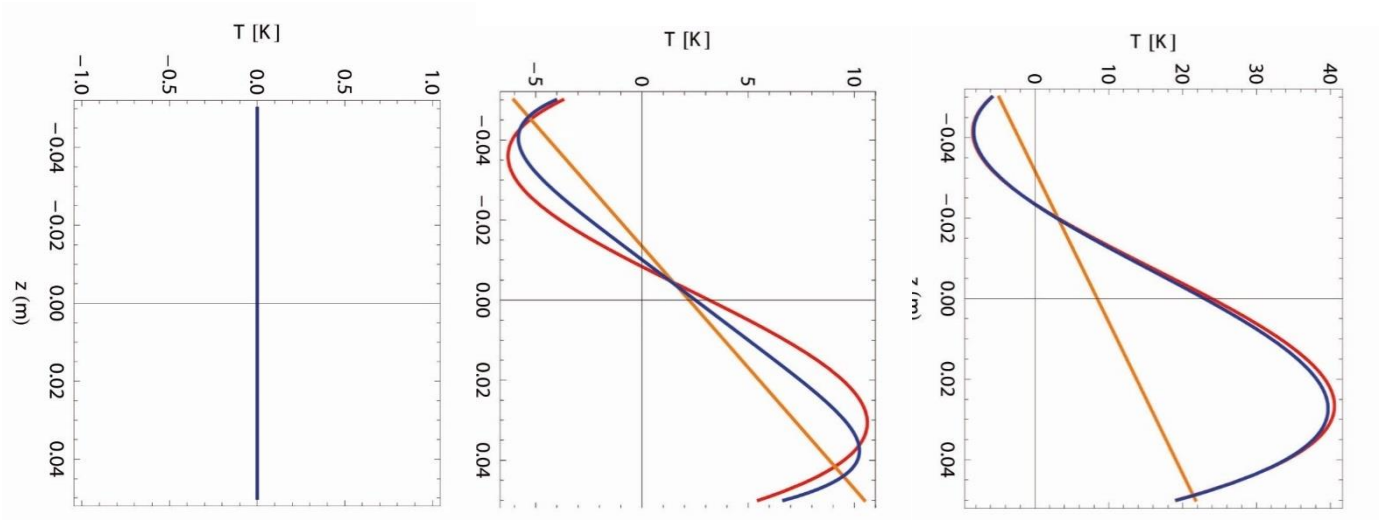

(a) (b) (c)

Figure 15. Temperature profiles, along *z* (thickness) direction, in the central point ($x = a/2$, $y = b/2$), at instants $t = 0$ s (a), $t = 100$ s (b),, and $t = 6000$ s (c),. $h = 0.1$ m . Colours (on-line): TTC-0D (red), STC-0D (blue) and CTC-0D (orange) models.

5. Effects of thermal modelling on nonlinear mechanical response

In the previous Section 4, non-stationary and stationary thermal regimes at continuum levels provided in post-processing by various zero-dimensional thermomechanical models have been evaluated.

In the complex and computationally burdensome context of nonlinear dynamics, it is clearly of great importance to select the possibly cheapest model still allowing to reliably describe the essential characteristics of the specific nonlinear phenomenon under examination. Thus, it is worth discussing how much thermal modelling affects the mechanical response in nonlinear dynamics. Below are some hints on the matter.

Both TTC-0D and CTC-0D models have only one mechanical balance equation with membrane-bending couplings (Eq.(3a)). Considering a plate in the same thermal boundary conditions of Sect. 4.3 (free heat exchange on up/down faces and cold edges), such equation in terms of configuration variables has the same structure for the two models, yet with simpler coefficients for CTC-0D ([32] and [33]):

$$a_{11}\ddot{W} + a_{12}\dot{W} + a_{13}W + a_{14}W^3 + a_{15}T_{R1} + a_{16}T_{R0}W + a_{17}f(t) = 0 \quad \text{(TTC-0D)} \tag{21}$$

$$b_{11}\ddot{W} + b_{12}\dot{W} + b_{13}W + b_{14}W^3 + b_{15}T_{R1} + b_{16}T_{R0}W + b_{17}f(t) = 0 \quad \text{(CTC-0D)} \tag{22}$$

where $W(t)$ is the deflection in the centre of the plate, T_{R0} and T_{R1} are the thermal variables of the models, and $f(t)$ is the mechanical excitation source.

The STC-0D model has mechanical balance equations depending on the expansion order assumed for the transverse displacement. If displacement terms of order higher than cubic are neglected (which is a suitable assumption for thin plates, where shear deformability does not play a decisive role), the mechanical balance of also STC-0D can be reduced to a single equation. Without going into more details because this model will not be used in the following, the structure of this single equation reads:

$$c_{11}\ddot{W} + c_{12}\dot{W} + c_{13}W + c_{14}W^3 + c_{15}T_{R1} + c_{16}T_{R3} + c_{17}T_{R5} + \left(c_{18}T_{R0} + c_{19}T_{R2} + c_{110}T_{R4}\right)W + c_{111}f(t) = 0 \quad \text{(STC-0D)} \tag{23}$$

Reduced temperature variables $T_{Ri}(t)$ are seen to affect the mechanical equations (21-23) through both parametric- and external-like excitation terms. Under the same physical conditions, these terms vary in number and intensity by changing the model, and their importance also depends on the values of corresponding coefficients (which change with the model, as well). Their nonlinear mechanical effects have to be evaluated. As to the drastic option of taking into account only the mean steady values of the thermal variables provided by the various models, by neglecting the underlying non-stationary regimes, previous works [35] have highlighted the crucial role played by the thermal transient evolution in steadily modifying the response of the mechanical system, already when using the simple CTC model. Thus, the whole thermal response (both non-stationary and stationary) has to be considered.

With the numerical values of the last subcase in Sect. 4.3 (thickness $h = 0.01\,\text{m}$, source energy $e^{(0)} = 8\times10^5\ \text{W/m}^3$ and $e^{(1)} = 1.15\times10^9\ \text{W/m}^4$), significant deviations of the temperature profiles of CTC-0D with respect to the practically coinciding ones of TTC-0D and STC-0D were pointed out. Therefore, in this case it may be sufficient to consider TTC-0D as a reference model (instead of STC-0D, which is more involved also in mechanical terms, see Eq. (23)) for comparing the mechanical behaviour of the simpler CTC one. The mentioned thermal deviations are due to the different time histories of the reduced variables T_{R0} and T_{R1} for the two models, which are overlapped in Fig.16.

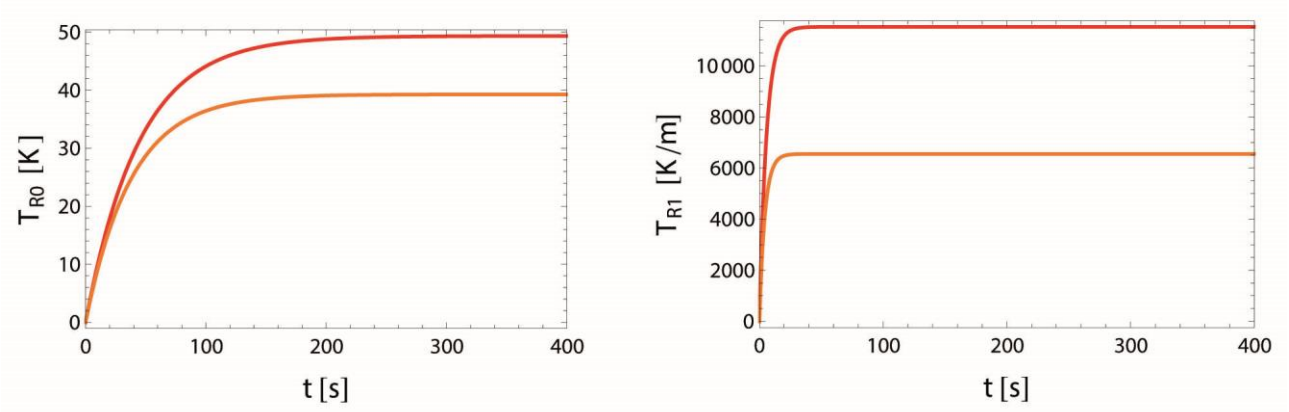

Figure 16. Time history of the membrane and bending thermal variables of TTC-0D and CTC-0D models, with material and thermal conditions of Sect. 4.3, and values: $h = 0.01$ m , $e^{(0)} = 8\times10^{5}$ W/m^3 e $e^{(1)} = 1.15\times10^{9}$ W/m^4. Colours (on-line): TTC-0D (red) and CTC-0D (orange) models.

To evaluate the effects of these different thermal responses on the mechanical outcomes of Eqs. (21) and (22), let us consider the case of movable edges [32, 35] subjected to uniform stretching forces of magnitudes $p_x = p_y = p$ in x and y direction (see Fig. 2), and transversal resonant harmonic forcing $f(t) = f\cos(\Omega t)$. The material's elastic properties are:

$$Y_1 = 1.72\cdot10^{11}\frac{N}{m^2},\quad \nu_{12} = 0.25,\quad Y_2 = 6.91\cdot10^{9}\frac{N}{m^2},\quad G_{12} = 3.45\cdot10^{9}\frac{N}{m^2},\quad \delta = 330\frac{N^*s}{m^3}$$

To deal with non-dimensional variables, the following transformations are applied:

$$W(t) = \bar{W}(t)h, \qquad T_{R0}(t) = \frac{h^2}{a^2\alpha_1}\bar{T}_{R0}(t), \qquad T_{R1}(t) = \frac{h}{a^2\alpha_1}\bar{T}_{R1}(t), \qquad \tau = \Omega t.$$

The subsequent system of non-dimensional equations for the plate motion reads (the over-bar upon the variables has been dropped for convenience):

$$\ddot{W} + a_{12}\dot{W} + a_{13}W + a_{14}W^3 + a_{15}T_{R1} + a_{16}W\ T_{R0} + a_{17}\cos(t) = 0 \tag{24a}$$

$$\dot{T}_{R0} + a_{22}T_{R0} + a_{23}\alpha_1 T_\infty + a_{24}W\dot{W} + a_{25} = 0 \tag{24b}$$

$$\dot{T}_{R1} + a_{32}T_{R1} + a_{33}\dot{W} + a_{34} = 0 \tag{24c}$$

Equations (24) govern the dynamical behaviour of both CTC and TTC, of course with different expressions of the nondimensional coefficients a_{ij} due to the diverse mechanical and thermal assumptions. For the plate under analysis, the relevant numerical values are:

CTC-0D

$$a_{12} = 0.059,\ a_{13} = 1 - p,\ a_{14} = 0.683,\ a_{15} = -0.367,\ a_{16} = -0.966,\ a_{17} = -f,\ a_{22} = 9.11\ 10^{-5},$$
$$a_{23} = -1.451,\ a_{24} = 1.01\ 10^{-4},\ a_{25} = -0.998\ e_0\ ,\ a_{32} = 7.87\ 10^{-4},\ a_{33} = 8.87\ 10^{-4},\ a_{34} = -12\ e_1$$

TTC-0D

$$a_{12} = 0.059,\ a_{13} = 1 - p,\ a_{14} = 0.686,\ a_{15} = -0.273,\ a_{16} = -0.904,\ a_{17} = -f,\ a_{22} = 7.81\ 10^{-5},$$
$$a_{23} = -1.239,\ a_{24} = 1.01\ 10^{-4},\ a_{25} = -1.07\ e_0,\ a_{32} = 6.06\ 10^{-4},\ a_{33} = 1.19\ 10^{-3},\ a_{34} = -16.2\ e_1$$

where p, f, e_0, e_1 are nondimensional parameters representing pretension, amplitude of mechanical excitation, membrane source energy and bending source energy, respectively. It is worth noting that Eqs. (24) are nondimensionalised with respect to the forcing frequency, which is set equal to the natural frequency of the plate in order to study the dynamical response in the neighbourhood of the primary resonance condition. Indeed, such condition is known to be the most critical one for the system in terms of amplification of the mechanical response to the applied (mechanical, but also thermal) excitation, and it is thus the most favourable state to capture possible effects due to the applied thermal energies. Of course, the two linear natural frequencies (without pretension application) of CTC and TTC models, which are dependent on the mechanical assumptions, slightly differ from each other ($\omega_{\mathrm{CTC}} = 287.4\ Hz$, $\omega_{\mathrm{TTC}} = 286.7\ Hz$), so that the following analyses compare the nondimensional responses of the two models around the relevant primary resonance conditions. As regards mechanical excitations, the plate is forced to be in an incipient buckling condition (corresponding to a pretension $p = 9860\ N/m^2$) and to undergo a weak harmonic excitation (of amplitude $f = 203\ kN/m$) able to trigger periodic responses, without however overwhelming the effect of thermal forcing.

To verify the effect of active thermal excitations e_0 and e_1 on the mechanical response, attention is focused on the system global behaviour, which is known to play a fundamental role in unveiling the full dynamics ensuing from the coexistence of fast (mechanical) and slow (thermal) phenomena [35]. 4D basins of attraction of the two models are investigated, by looking at relevant 2D cross-sections in the mechanical plane for fixed thermal initial conditions. Figure 17a,b shows the comparison of CTC and TTC global outcomes when the evolution of thermal variables starts from null values, which represents the most natural condition from a physical viewpoint. Both models display an almost identical monostable scenario (gray basins), characterized by the 1-period pre-buckling solution represented in terms of time history and phase portrait in Fig. 17c,d. However, it is of interest analysing also the response of the relevant uncoupled systems, obtained by separately solving the uncoupled (i.e., a_{24}=a_{33}=0) thermal equations (24) and inserting the obtained mean steady values of the thermal variables T_{R0} and T_{R1} into the mechanical equation. The relevant 2D basins of attraction are reported in Fig. 18a,b and display another (blue) basin corresponding to a buckled response described in Fig. 18c,d, which becomes the dominant solution for both CTC and TTC uncoupled systems, and the magenta basin relevant to a period-2 solution. The results show small differences in the basins size of the gray (pre-buckling), blue (buckled) and magenta (period-2) responses of the uncoupled systems. More importantly, significant differences are pointed out by comparing outcomes from the coupled (Fig. 17) and uncoupled (Fig. 18) models, which highlight the major role played by the thermal transient in determining the steady mechanical response of thermomechanical models. In fact, when it is neglected, as in the uncoupled cases, the effect of thermal excitations in terms of variation of membrane and bending temperatures is entirely and immediately incorporated into the mechanical equation, allowing the system to settle onto a buckled configuration at once.

Conversely, the coupled models naturally account for the temporal evolution of the thermal variables, which furnish a slow contribution to the mechanical vibrations by means of the coupling terms. At the same time, the mechanical evolution develops much quicker than the thermal one (as highlighted by Fig. 16 vs Figs. 17c and 18c), settling onto the stable (pre-buckling) response long before the thermal evolution has provided its full contribution.

The above results highlight the role played by the simultaneous presence of slow and fast dynamics in coupled thermomechanical models, which is definitely dominant with respect to that of possibly different modelling assumptions of thermal behaviour, and such to make the features of the mechanical response provided by also the simplest (CTC) minimal model substantially equivalent to those obtainable with most refined (i.e., TTC and higher-order) thermal models. In this respect, it is worth noting that the presented results refer to a thin plate, for which the refined temperature function of the TTC-0D model has certainly a minor effect compared to what would happen for thick plates.

However, in this latter case, it would be rather difficult to distinguish differences in the mechanical response due to different thermal assumptions from those certainly arising due to different mechanical assumptions, which are also present in the TTC model (owed to the shear deformability hypothesis) and likely to play the fundamental role. In any case, non-trivial differences can be produced by different thermal assumptions in the transient and (mostly) steady thermal regimes of also thin plates, as previously noticed (see Fig. 16). Accordingly, it is necessary to refer to at least the TTC-0D model - which is also much more flexible in accounting for thermal boundary conditions - for reliably describing both thermal and mechanical responses.

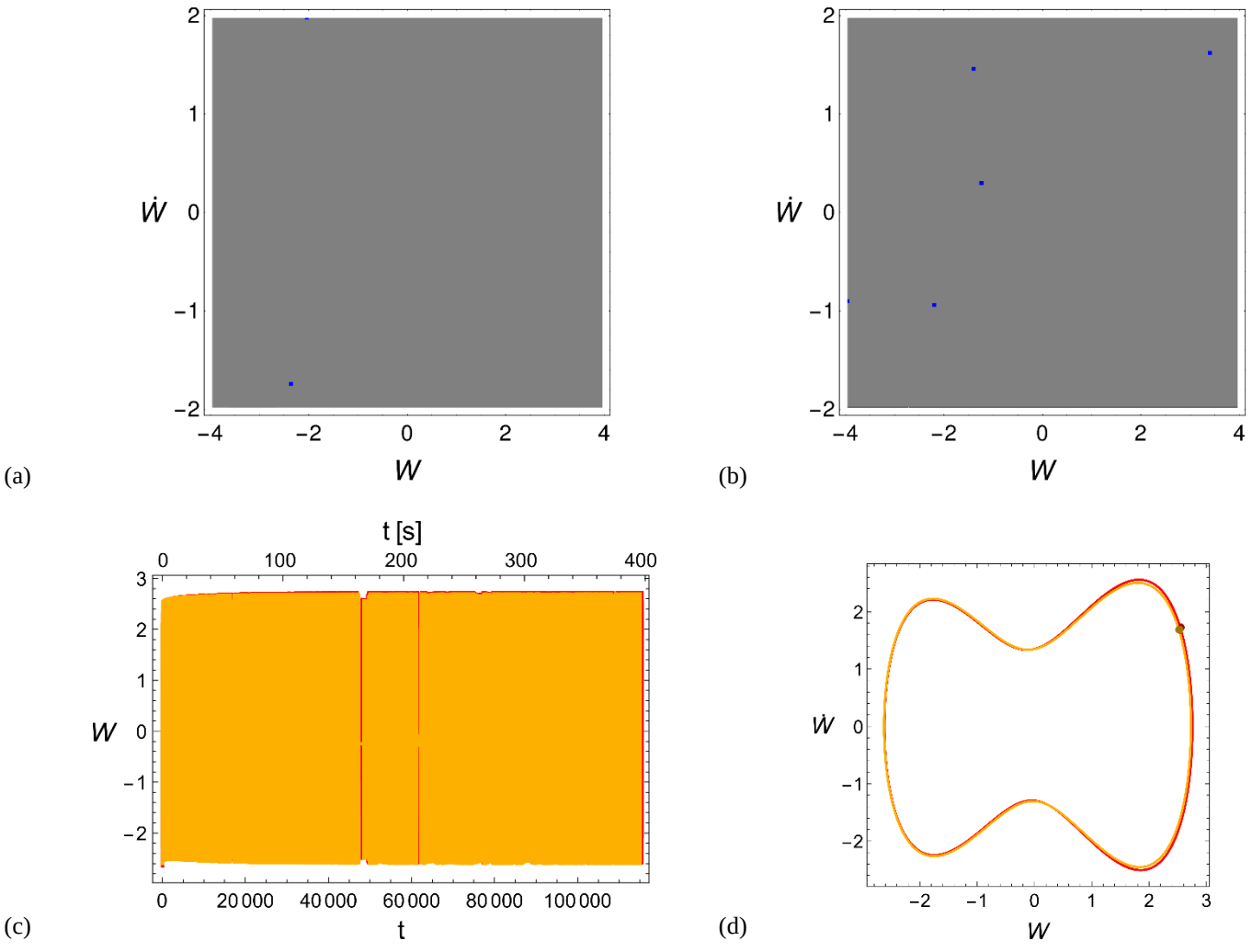

Figure 17. Cross-sections of the 4D basins of attraction of the thermomechanical models CTC-0D (a) and TTC-0D (b) in the $(W,\dot{W})$ plane, with $T_{R0}(0)=T_{R1}(0)=0$. Temporal evolutions (c) and phase portraits (d) of the gray basin 1-period solution. Red solution: TTC response, Orange solution: CTC response.

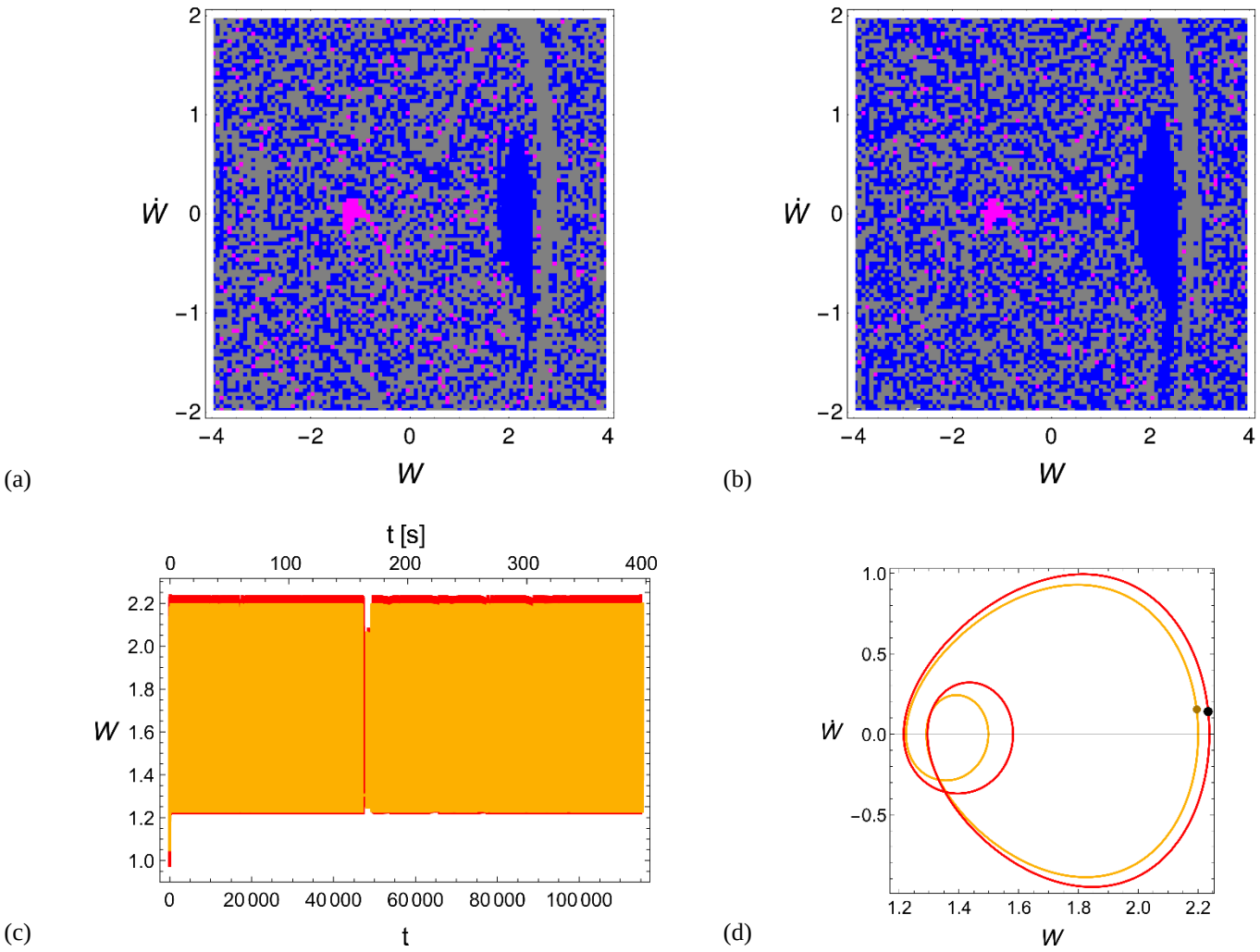

Figure 18. Basins of attraction of the uncoupled thermomechanical models CTC-0D (a) and TTC-0D (b) in the $(W,\dot{W})$ plane. Temporal evolutions (c) and phase portraits (d) of the blue basin 1-period solution. Red solution: TTC response, blue solution: CTC response.

5. Conclusions

Minimal thermal modelling of two-way thermomechanically coupled plates has been addressed in the background of a unified and consistent formulation of the underlying continuum problem. Upon presenting variably refined reduced-order thermal models, some main features of the response to active thermal sources of isotropic or orthotropic plates with different materials have been investigated in both transient and steady regime. Moving from the results provided by the reduced-order models, attention has been focused on the reconstruction of 3D temperature configurations and energy balances, controllably pursued in the framework of the accomplished 3D $\rightarrow$ 0D dimension reduction of the thermomechanical problem, by also comparing outcomes with those of analytical solutions available from the literature. For the richer models allowing to account for the presence of a meaningful variety of thermal boundary conditions, in addition to body thermal excitations, different combinations of boundary/body sources have been considered in order to get a reasonably reliable evaluation of the relevant advantages and limitations.

From the whole set of obtained results, a Third-order Thermomechanically Coupled (TTC) minimal model – consistently complementing the third-order assumption of transverse displacement suitable to deal

with also shear-deformable 2D composites with a correspondingly assumed cubic temperature distribution along the thickness – has shown to be overall reliable as regards the thermal response. Indeed, in comparison with both a richer reduced model characterized by an assumed seventh-order temperature distribution (STC) and analytical solutions, where available, it succeeds in providing not only the same steady temperature in the plate centre and correspondingly similar distributions along transverse direction and mid-plane symmetry axes, but also a reasonable description of the transient dynamics which only exhibits a non-realistic temperature overestimation in the first instants of the time evolution. With respect to the more refined STC model, TTC has the advantages of being the minimal reduced model (only two thermal ODEs, instead of six) which still allows to consider a wide variety of boundary and body thermal excitations of technical interest, with a capability to comprehensively describe thermal regimes.

This appears of particular interest also in view of pursuing in the cheapest possible way from the thermal viewpoint a systematic, yet computationally demanding, investigation of the nonlinear dynamic response of the actually coupled thermomechanical plate to a combination of mechanical and thermal excitations. In this respect, while referring all the way to the minimal modelling also from the mechanical viewpoint (one ODE in the sole transverse displacement, suitable to address cases of no internal resonance), it is of course necessary to get indications about the influence of the degree of refinement of thermal modelling on the mechanical outcomes of the thermomechanically coupled response.

This has been accomplished in the final part of the paper by considering a thermal excitation condition of a mechanically buckled plate, in addition to harmonic transverse mechanical excitation, which can be studied via an even simpler reduced model (Classical Thermomechanically Coupled, CTC) exhibiting the same minimal number of three ODEs, however suitable to deal only with thin 2D composites. Mechanical outcomes of TTC and CTC have been compared with each other via a global dynamics analysis allowing to highlight the influence of the slow thermal transient on the steady outcomes of the faster mechanical response, which was previously shown to be the most meaningful effect of full thermomechanical coupling on the mechanical response, already detectable by the simpler CTC model. Using TTC instead of CTC has been seen to provide only quantitative, and relatively minor, differences on the mechanical outcomes while, of course, the thermal outcomes are substantially different in the two cases in both transient and steady regimes, as highlighted in the main body of the paper.

So, if being mainly interested in the mechanical aspects of the dynamics, even the simpler minimal CTC model could be reliably used, in principle. However, and irrespective of being possibly uninterested in the associated thermal outcomes (which would sound anyway questionable in itself), this only holds for the quite particular condition of free heat exchange through the boundary surface, to be solely addressed if using the CTC model. Thus, investigating the two-way coupled thermomechanical response under more general combinations of active thermal excitations, in addition to mechanical ones, requires using the minimal TTC model, with a reasonable confidence as regards the overall reliability of the ensuing results. This is indeed the subject of a companion paper [42].

Acknowledgements The financial support of Italian research program PRIN 2015 (No. 2015JW9NJT) is acknowledged.

References

[1] Manoach E, Ribeiro P. Coupled, thermoelastic, large amplitude vibrations of Timoshenko beam. Int J Mech Sci 2004; 46(11):1589–606.

[2] Ribeiro P, Manoach E. The effect of temperature on the large amplitude vibrations of curved beams. J Sound Vib 2005; 285(4–5):1093–107.

[3] Warminska A, Manoach E, Warminski J., Nonlinear dynamics of a reduced multimodal Timoshenko beam subjected to thermal and mechanical loadings. Meccanica 2014; 49(8):1775–93.
[4] Warminska A, Manoach E, Warminski J, Samborski S. Regular and chaotic oscillations of a Timoshenko beam subjected to mechanical and thermal loadings. Cont Mech Thermodyn 2015; 27(4–5):719–37.
[5] Lee, J., 1993, Large-amplitude plate vibration in an elevated thermal environment, Appl Mech Rev, 46, pp. S242-S254
[6] Shi Y, Lee RYY, Mei C. Thermal postbuckling of composite plates using the finite element modal coordinate method. J Therm Stresses 1999:595–614.
[7] Ribeiro P. Thermally induced transitions to chaos in plate vibrations. J Sound Vib 2007; 299(1–2):314–30.
[8] Zhang W, Yang J, Hao Y. Chaotic vibrations of an orthotropic FGM rectangular plate based on third-order shear deformation theory. Nonlin Dyn 2010; 59:619–60.
[9] Alijani F, Bakhtiari-Nejad F, Amabili M. Nonlinear vibrations of FGM rectangular plates in thermal environments. Nonlin Dyn 2011; 66(3):251–70.
[10] Amabili M, Tajahmadi Mohammad Reza Sareban. Thermal post-buckling of laminated and isotropic rectangular plates with fixed edges: comparison of experimental and numerical results. Proc Inst Mech Eng Part C 2012; 226(10):2393–401
[11] Manoach, A. Warminska, J. Warminski, S. Doneva: A reduced multimodal thermoelastic model of a circular Mindlin plate. Int J Mech Sci 153–154 (2019) 479–489.
[12] Spottswood, S.M., Hollkamp, J.J. and Eason, T.G., Reduced-order models for a shallow curved beam under combined loading, AIAA Journal (2010) 48(1): 47-55.
[13] Perez, R., Wang, X.Q., and Mignolet, M.P., 2011, Nonlinear reduced-order models for thermoelastodynamic response of isotropic and functionally graded panels, AIAA Journal, 49, pp. 630-641.
[14] S Jain, P Tiso: Model order reduction for temperature-dependent nonlinear mechanical systems: a multiple scales approach. arXiv preprint arXiv:1903.02073, 2019.
[15] Allen, D.H. (1991) Thermomechanical coupling in inelastic solids. Appl Mech Rev 44, 361-373.
[16] Karagiozova, D., Manoach, E. (1992) Coupling effect in an elastic-plastic beam subjected to heat impact. Nucl Engng Des 135, 267-276.
[17] Shin, E.-S. and Kim, S.J. (1997) Quantitative prediction of thermomechanical coupling effect in thermo–elasto–viscoplastic composite materials. AIAA Journal 35, 1746-1752.
[18] Senchenkov, I.K and Andrushko, N.F. (2006) Thermomechanical coupling effects in a materially nonlinear disk under impulsive radial loading Int Appl Mech 42, 951-958.
[19] Bednarcyk B.A., Aboudi J., Arnold S.M., Pineda E.J.: A multiscale two-way thermomechanically coupled micromechanics analysis of the impact response of thermo-elastic-viscoplastic composites, Int J Solids Structures, 161, 228-242, 2019.
[20] Daneshjo K, Ramezani M. Classical coupled thermoelasticity in laminated composite plates based on third-order shear deformation theory. Compos Struct 2004; 64(3–4):369–75.
[21] Lezgy-Nazargah, M. (2015) Fully coupled thermo-mechanical analysis of bi-directional FGM beams using NURBS isogeometric finite element approach. Aerosp Sci Techn 45, 154-164.
[22] Brischetto S, Carrera E. Coupled thermo-mechanical analysis of one-layered and multi-layered plates. Compos Struct 2010; 92(8):1793–812.
[23] Fazzolari, F.A. and Carrera, E. (2014) Coupled thermoelastic effect in free vibration analysis of anisotropic multilayered plates and FGM plates using a variable-kinematics Ritz formulation. Eur J Mech – A/Solids 44, 157-174.
[24] Carrera, E., Fazzolari, F.A., and Cinefra, M. (2017) Thermal Stress Analysis of Composite Beams, Plates and Shells, Elsevier, New York.
[25] Chang WP, Wan SM. Thermomechanically coupled non-linear vibration of plates. Int J Non-Linear Mech 1986;21(5):375–89.
[26] Chang, W.P., Jen, S., 1986, Nonlinear free vibration of heated orthotropic rectangular plates, Int J Solids Structures, 22, 267-281.
[27] Shu X, Zhang X, Zhang J. Thermoelastic free vibration of clamped circular plate. Appl Math Mech 2000;21(6):715–24.
[28] Yeh Y-L. Chaotic and bifurcation dynamic behavior of a simply supported rectangular orthotropic plate with thermo-mechanical coupling. Chaos Solit Fract 2005;24:1243–55.

[29] Yeh Y-L. The effect of thermo-mechanical coupling for a simply supported orthotropic rectangular plate on non-linear dynamics. Thin-Walled Struct 2005;43:1277–95.
[30] Goodpaster B.A., Harne R.L.: Analytical modeling and impedance characterization of the nonlinear dynamics of thermomechanically coupled structures. J. Appl. Mech., 85, 081010-1-9, 2018
[31] Saetta, E.; Rega, G.: Unified 2D continuous and reduced order modelling of thermomechanically coupled laminated plate for nonlinear vibrations. Meccanica, 49(8), 1723-1749, 2014.
[32] Saetta, E.; Rega, G.: Third-order thermomechanically coupled laminated plates: 2D nonlinear modelling, minimal reduction and transient/post-buckled dynamics under different thermal excitations. Compos Struct, 174, 420-441, 2017.
[33] Tonti, E.: The Mathematical Structure of Classical and Relativistic Physics. Birkhäuser-Springer, 2013.
[34] Settimi, V.; Saetta, E.; Rega, G.: Local and global nonlinear dynamics of thermomechanically coupled laminated plates in passive thermal regime. Nonlin Dyn, Vol. 93, No. 1, pp. 167-187, 2018.
[35] Settimi, V.; Rega, G.; Saetta, E.: Avoiding/inducing dynamic buckling in a thermomechanically coupled plate: A local and global analysis of slow/fast response. Proc Roy Soc A, 474, 2213, 20180206, 2018.
[36] Rega, G.; Saetta, E.: Shear deformable composite plates with nonlinear curvatures: Modeling and nonlinear vibrations of symmetric laminates. Arch Appl Mech, 82, 1627–1652, 2012.
[37] Saetta E, Rega G, Modelling, dimension reduction, and nonlinear vibrations of thermomechanically coupled laminated plates. Proc Engng 2016;144:875–882.
[38] Nowacki W. Dynamic Problems of Thermoelasticity, PWN-Polish Scientific Publishers, Warszawa, 1975
[39] V.B.Tungikar, Koganti M. Rao Three-dimensional exact solution of thermal stresses in rectangular composite laminate. Compos Struct, 27(4), 1994, 419-430.
[40] A.V. Luikov Analytical Heat Diffusion Theory, Academic Press, 1968.
[41] Settimi V., Rega G. (2019), Thermomechanical coupling and transient to steady global dynamics of orthotropic plates, in Problems of Nonlinear Mechanics and Physics of Materials (Eds. I. V. Andrianov et al.), Springer Series “Advanced Structured Materials”, Springer, v. 94, pp. 483-499.
[42] Settimi, V., Saetta, E., Rega, G., Nonlinear dynamics of a third-order reduced model of thermomechanically coupled plate under different thermal excitations. (2019) (submitted)

Supplementary material from **Minimal thermal modelling of two-way thermomechanically coupled plates for nonlinear dynamics investigation**

A. Non-stationary conduction analytical solution

In the case of non-stationary conduction, the differential heat equation for an isotropic solid in the absence of source energy and with all the 6 external faces at constant temperature is analytically satisfied by the following temperature field in convergent series form [40]:

$$T(x,y,z,t) = -T^* \sum_{n=1}^{\infty}\sum_{m=1}^{\infty}\sum_{k=1}^{\infty} A_n A_m A_k \cos\left(\frac{\mu_n}{R_1}(x-a/2)\right)\cos\left(\frac{\mu_m}{R_2}(y-b/2)\right)\cos\left(\frac{\mu_k}{R_3}z\right) \times \exp[-\left(\mu_n^2 K_1^2 + \mu_m^2 K_2^2 + \mu_k^2 K_3^2\right)\mathrm{F}_0] + T^* \tag{A.1}$$

where: $A_n = (-1)^{n+1}\frac{2}{\mu_n}$; $A_m = (-1)^{m+1}\frac{2}{\mu_m}$; $A_k = (-1)^{k+1}\frac{2}{\mu_k}$; $\mu_n = (2n-1)\frac{\pi}{2}$; $\mu_m = (2m-1)\frac{\pi}{2}$; $\mu_k = (2k-1)\frac{\pi}{2}$; $K_i = \frac{R}{R_i}$ $(i = 1,2,3)$ with $R_1 = a/2$, $R_2 = b/2$, $R_3 = h/2$ and R generalized size where $\frac{1}{R^2} = \frac{1}{R_1^2} + \frac{1}{R_2^2} + \frac{1}{R_3^2}$; $F_0 = \frac{1}{R^2}\frac{\lambda}{\rho c_v}t$ (Fourier number) with λ thermal conductivity, ρ mass density, c_v specific heat at constant strain, t time; T^* temperature on the external faces.

B. Stationary conduction analytical solution

In the case of stationary conduction, the differential heat equation for an orthotropic solid in the absence of source energy is analytically satisfied by the following temperature field [39]:

$$T(x,y,z) = \left(C_1 \sinh(s_1 z) + C_2 \cosh(s_1 z)\right)\sin(\alpha x)\sin(\beta y) \tag{B.1}$$

where: $\alpha = m\pi/a$ and $\beta = m\pi/b$, with m and n number of waves, a and b dimension of the rectangular plate; $s_{1,2} = \pm\sqrt{\frac{\lambda_{11}\alpha^2 + \lambda_{22}\beta^2}{\lambda_{33}}}$ with λ_{ij} thermal conductivities; C_1 and C_2 constants that depend on the boundary conditions.

C. Coefficients of Eqs.(10), (13), and (18)

Coefficients of Eqs.(12a,b):

$$a_{21}=-\frac{1}{6}abh\rho c_v,\quad a_{22}=-\frac{h\pi^2\left(b^2\lambda_{11}+a^2\lambda_{22}\right)}{6ab}-\frac{2ab\lambda_{33}}{h},\quad a_{23}=\frac{16ab\lambda_{33}}{h\pi^2},\ a_{25}=\frac{abh}{4}$$

$$a_{31}=-\frac{2abh^3\rho c_v}{15\pi^2},\quad a_{32}=-\frac{8abh\lambda_{33}}{\pi^2},\quad a_{34}=\frac{1}{48}abh^3 \tag{C.1}$$

Coefficients of Eqs.(15a,b):

$$a_{21}=-\frac{1}{5}abh\rho c_v,\quad a_{22}=-\frac{h\pi^2\left(b^2\lambda_{11}+a^2\lambda_{22}\right)}{5ab}-\frac{6ab\lambda_{33}}{5h},\quad a_{23}=\frac{1}{60}abh^2\rho c_v,\quad a_{28}=\frac{abh}{4},$$

$$a_{24}=\frac{h^2\pi^2\left(b^2\lambda_{11}+a^2\lambda_{22}\right)}{60ab}-\frac{2}{5}ab\lambda_{33},\quad a_{25}=-\frac{ab}{5}+\frac{h^2\pi^2\left(b^2\lambda_{11}+a^2\lambda_{22}\right)}{120ab\lambda_{33}},\quad a_{26}=-\frac{h\pi^2\left(b^2\lambda_{11}+a^2\lambda_{22}\right)}{20ab}+\frac{6}{5}ab\lambda_{33},$$

$$a_{31}=\frac{1}{100}abh^2\rho c_v,\quad a_{32}=\frac{h^2\pi^2\left(b^2\lambda_{11}+a^2\lambda_{22}\right)}{100ab}-\frac{2}{5}ab\lambda_{33},\quad a_{33}=-\frac{1}{75}abh^3\rho c_v,\quad a_{38}=\frac{1}{48}abh^3 \tag{C.2}$$

$$a_{34}=-\frac{h^3\pi^2\left(b^2\lambda_{11}+a^2\lambda_{22}\right)}{75ab}-\frac{3}{10}abh\lambda_{33},\quad a_{35}=\frac{abh}{10}-\frac{h^3\pi^2\left(b^2\lambda_{11}+a^2\lambda_{22}\right)}{400ab\lambda_{33}},\ a_{36}=-\frac{h^2\pi^2\left(b^2\lambda_{11}+a^2\lambda_{22}\right)}{100ab}+\frac{2}{5}ab\lambda_{33}$$

Coefficients of Eqs.(20a,b):

$$a_{21}=-\frac{abh\rho c_v\left(hH+6\lambda_{33}\right)}{6\left(hH+4\lambda_{33}\right)},\quad a_{22}=-\frac{b^2h\pi^2\lambda_{11}\left(hH+6\lambda_{33}\right)+a^2\left(12b^2H\lambda_{33}+h\pi^2\lambda_{22}\left(hH+6\lambda_{33}\right)\right)}{6ab\left(hH+4\lambda_{33}\right)},$$

$$a_{23}=-\frac{h^2H\pi^2\left(b^2\lambda_{11}+a^2\lambda_{22}\right)-24a^2b^2H\lambda_{33}}{12ab\left(hH+4\lambda_{33}\right)},\quad a_{25}=\frac{abh}{4},\quad a_{31}=-\frac{abh^3\rho c_v\left(hH+12\lambda_{33}\right)}{120\left(hH+6\lambda_{33}\right)}, \tag{C.3}$$

$$a_{32}=-\frac{h\left(\left(b^2h^2\pi^2\lambda_{11}+a^2h^2\pi^2\lambda_{22}\right)\left(hH+12\lambda_{33}\right)+a^2\left(60b^2\lambda_{33}\left(hH+2\lambda_{33}\right)\right)\right)}{120ab\left(hH+6\lambda_{33}\right)},\quad a_{34}=\frac{1}{48}abh^3$$

D. Governing equations of the STC-0D model

Case 1 (Sect.4.1):

$$
\begin{aligned}
&a_{21}\dot{T}_{R0}+a_{22}T_{R0}+a_{23}\dot{T}_{R2}+a_{24}T_{R2}+a_{25}\dot{T}_{R4}+a_{26}T_{R4}+2a_{27}T^{*}+a_{29}e^{(0)}(t)=0\\
&a_{31}\dot{T}_{R1}+a_{32}T_{R1}+a_{33}\dot{T}_{R3}+a_{34}T_{R3}+a_{35}\dot{T}_{R5}+a_{36}T_{R5}+a_{38}e^{(1)}(t)=0\\
&a_{41}\dot{T}_{R0}+a_{42}T_{R0}+a_{43}\dot{T}_{R2}+a_{44}T_{R2}+a_{45}\dot{T}_{R4}+a_{46}T_{R4}+2a_{47}T^{*}+a_{49}e^{(2)}(t)=0\\
&a_{51}\dot{T}_{R1}+a_{52}T_{R1}+a_{53}\dot{T}_{R3}+a_{54}T_{R3}+a_{55}\dot{T}_{R5}+a_{56}T_{R5}+a_{58}e^{(3)}(t)=0\\
&a_{61}\dot{T}_{R0}+a_{62}T_{R0}+a_{63}\dot{T}_{R2}+a_{64}T_{R2}+a_{65}\dot{T}_{R4}+a_{66}T_{R4}+2a_{67}T^{*}+a_{69}e^{(4)}(t)=0\\
&a_{71}\dot{T}_{R1}+a_{72}T_{R1}+a_{73}\dot{T}_{R3}+a_{74}T_{R3}+a_{75}\dot{T}_{R5}+a_{76}T_{R5}+a_{78}e^{(5)}(t)=0
\end{aligned}
\tag{D.1}
$$

Case 2 (Sect.4.2):

$$
\begin{aligned}
&a_{21}\dot{T}_{R0}+a_{22}T_{R0}+a_{23}\dot{T}_{R1}+a_{24}T_{R1}+a_{25}\dot{T}_{R2}+a_{26}T_{R2}+a_{27}\dot{T}_{R3}+a_{28}T_{R3}+a_{29}\dot{T}_{R4}+a_{210}T_{R4}\\
&+a_{211}\dot{T}_{R5}+a_{212}T_{R5}+a_{213}q^{*}+a_{214}T^{*}+a_{216}e^{(0)}(t)=0\\
&a_{31}\dot{T}_{R0}+a_{32}T_{R0}+a_{33}\dot{T}_{R1}+a_{34}T_{R1}+a_{35}\dot{T}_{R2}+a_{36}T_{R2}+a_{37}\dot{T}_{R3}+a_{38}T_{R3}+a_{39}\dot{T}_{R4}+a_{310}T_{R4}\\
&+a_{311}\dot{T}_{R5}+a_{312}T_{R5}+a_{313}q^{*}+a_{314}T^{*}+a_{316}e^{(1)}(t)=0\\
&a_{41}\dot{T}_{R0}+a_{42}T_{R0}+a_{43}\dot{T}_{R1}+a_{44}T_{R1}+a_{45}\dot{T}_{R2}+a_{46}T_{R2}+a_{47}\dot{T}_{R3}+a_{48}T_{R3}+a_{49}\dot{T}_{R4}+a_{410}T_{R4}\\
&+a_{411}\dot{T}_{R5}+a_{412}T_{R5}+a_{413}q^{*}+a_{414}T^{*}+a_{416}e^{(2)}(t)=0\\
&a_{51}\dot{T}_{R0}+a_{52}T_{R0}+a_{53}\dot{T}_{R1}+a_{54}T_{R1}+a_{55}\dot{T}_{R2}+a_{56}T_{R2}+a_{57}\dot{T}_{R3}+a_{58}T_{R3}+a_{59}\dot{T}_{R4}+a_{510}T_{R4}\\
&+a_{511}\dot{T}_{R5}+a_{512}T_{R5}+a_{513}q^{*}+a_{514}T^{*}+a_{516}e^{(3)}(t)=0\\
&a_{61}\dot{T}_{R0}+a_{62}T_{R0}+a_{63}\dot{T}_{R1}+a_{64}T_{R1}+a_{65}\dot{T}_{R2}+a_{66}T_{R2}+a_{67}\dot{T}_{R3}+a_{68}T_{R3}+a_{69}\dot{T}_{R4}+a_{610}T_{R4}\\
&+a_{611}\dot{T}_{R5}+a_{612}T_{R5}+a_{613}q^{*}+a_{614}T^{*}+a_{616}e^{(4)}(t)=0\\
&a_{71}\dot{T}_{R0}+a_{72}T_{R0}+a_{73}\dot{T}_{R1}+a_{74}T_{R1}+a_{75}\dot{T}_{R2}+a_{76}T_{R2}+a_{77}\dot{T}_{R3}+a_{78}T_{R3}+a_{79}\dot{T}_{R4}+a_{710}T_{R4}\\
&+a_{711}\dot{T}_{R5}+a_{712}T_{R5}+a_{713}q^{*}+a_{714}T^{*}+a_{716}e^{(5)}(t)=0
\end{aligned}
\tag{D2}
$$

Case 3 (Sect.4.3):

$$
\begin{aligned}
&a_{21}\dot{T}_{R0}+a_{22}T_{R0}+a_{23}\dot{T}_{R2}+a_{24}T_{R2}+a_{25}\dot{T}_{R4}+a_{26}T_{R4}+a_{27}T_{\infty}+a_{29}e^{(0)}(t)=0\\
&a_{31}\dot{T}_{R1}+a_{32}T_{R1}+a_{33}\dot{T}_{R3}+a_{34}T_{R3}+a_{35}\dot{T}_{R5}+a_{36}T_{R5}+a_{38}e^{(1)}(t)=0\\
&a_{41}\dot{T}_{R0}+a_{42}T_{R0}+a_{43}\dot{T}_{R2}+a_{44}T_{R2}+a_{45}\dot{T}_{R4}+a_{46}T_{R4}+a_{47}T_{\infty}+a_{49}e^{(2)}(t)=0\\
&a_{51}\dot{T}_{R1}+a_{52}T_{R1}+a_{53}\dot{T}_{R3}+a_{54}T_{R3}+a_{55}\dot{T}_{R5}+a_{56}T_{R5}+a_{58}e^{(3)}(t)=0\\
&a_{61}\dot{T}_{R0}+a_{62}T_{R0}+a_{63}\dot{T}_{R2}+a_{64}T_{R2}+a_{65}\dot{T}_{R4}+a_{66}T_{R4}+a_{67}T_{\infty}+a_{69}e^{(4)}(t)=0\\
&a_{71}\dot{T}_{R1}+a_{72}T_{R1}+a_{53}\dot{T}_{73}+a_{74}T_{R3}+a_{75}\dot{T}_{R5}+a_{76}T_{R5}+a_{78}e^{(5)}(t)=0
\end{aligned}
\tag{D3}
$$

E. Case 1 (Sect.4.1): exact closed form non-stationary solution of Eq. (2a) in terms of temperature

By expressing Eq.(4a) in terms of temperature for this case, eliminating source and thermomechanical contributions, we have [32]:

$$
\frac{2}{3}h\left(\lambda_{11}\frac{\partial^2 T_0}{\partial^2 x}+\lambda_{22}\frac{\partial^2 T_0}{\partial^2 y}-\rho c_v\frac{\partial T_0}{\partial t}\right)+\frac{8\lambda_{33}}{h}\left(T^*-T_0\right)=0 \tag{E.1}
$$

This equation is satisfied by the following solution:

$$
T_0(x,y,t)=T^*+\left(T_{R0}(t)-T^*\right)\sin\frac{\pi x}{a}\sin\frac{\pi y}{b}, \tag{E.2}
$$

which coincides with the dome-shape temperature distribution (7a) assumed in the 2D $\rightarrow$ 0D reduction, with

$$
T_{R0}(t)=c_0 e^{-\frac{\left(\pi^2\left(\frac{\lambda_{11}}{a^2}+\frac{\lambda_{22}}{b^2}\right)+\frac{12\lambda_{33}}{h^2}\right)}{\rho c_v}t}+T^* \tag{E.3}
$$

where constant c_0, particularized for $T_{R0}(0)=0$, is $c_0=-T^*$. Eq.(E.3) is also solution of Eq.(12a) without source terms.

F. Case 2 (Sect.4.2): exact closed form non-stationary solution of Eqs. (2) in terms of temperature

By expressing Eqs.(4) in terms of configuration for this case, eliminating source and thermomechanical contributions, we have [32]:

$$
\begin{aligned}
&\frac{4}{5}h\left(\lambda_{11}\frac{\partial^2 T_0}{\partial^2 x}+\lambda_{22}\frac{\partial^2 T_0}{\partial^2 y}-\rho c_v\frac{\partial T_0}{\partial t}\right)+\frac{4}{5}\lambda_{33}\left(\frac{6T^*}{h}-\frac{q^*}{\lambda_{33}}-\frac{6T_0}{h}-2T_1\right)=0\\
&\frac{4}{75}h^3\left(\lambda_{11}\frac{\partial^2 T_1}{\partial^2 x}+\lambda_{22}\frac{\partial^2 T_1}{\partial^2 y}-\rho c_v\frac{\partial T_1}{\partial t}\right)+\frac{2}{5}h\lambda_{33}\left(\frac{4T^*}{h}+\frac{q^*}{\lambda_{33}}-\frac{4T_0}{h}-3T_1\right)=0
\end{aligned}
\tag{F.1}
$$

This equations system is satisfied by the following solution:

$$T_0(x,y,t)=T_{R0}(t)\sin\frac{\pi x}{a}\sin\frac{\pi y}{b},\qquad T_1(x,y,t)=T_{R1}(t)\sin\frac{\pi x}{a}\sin\frac{\pi y}{b} \tag{F.2}$$

with

$$T_{R0}=\sqrt{2049}e^{\frac{-t\left(-\frac{4\pi^2\lambda_{11}}{a^2}-\frac{4\pi^2\lambda_{22}}{b^2}-\frac{\left(57+\sqrt{2049}\right)\lambda_{33}}{h^2}\right)}{4\rho c_v}}\left(12\left(\left(-33+\sqrt{2049}\right)c_0+8hc_1+e^{\frac{\sqrt{2049}t\lambda_{33}}{2h^2\rho c_v}}\right.\right.$$

$$\left.\left(\left(33+\sqrt{2049}\right)c_0-8hc_1\right)+\left(\frac{1}{24\sqrt{2049}}e^{\frac{t\left(\frac{4\pi^2\lambda_{11}}{a^2}+\frac{4\pi^2\lambda_{22}}{b^2}+\frac{\left(57+\sqrt{2049}\right)\lambda_{33}}{h^2}\right)}{4\rho c_v}}\left(2h^5\pi^4q^*\left(b^2\lambda_{11}+a^2\lambda_{22}\right)^2\right.\right.\right.$$

$$-3h^3\pi^2\left(b^2\lambda_{11}+a^2\lambda_{22}\right)\left(-5a^2b^2q^*+4h\pi^2T^*\left(b^2\lambda_{11}+a^2\lambda_{22}\right)\right)\lambda_{33}+90a^2b^2h\left(-20a^2b^2q^*$$

$$\left.\left.\left.+h\pi^2T^*\left(b^2\lambda_{11}+a^2\lambda_{22}\right)\right)\lambda_{33}^2+3600a^4b^4T^*\lambda_{33}^3\right)\right)/\left(\lambda_{33}\left(2h^4\pi^4\left(b^2\lambda_{11}+a^2\lambda_{22}\right)^2+57a^2b^2h^2\pi^2\right.\right.$$

$$\left.\left.\left(b^2\lambda_{11}+a^2\lambda_{22}\right)\lambda_{33}+150a^4b^4\lambda_{33}^2\right.\right.$$

$$T_{R1}=\frac{1}{8\sqrt{2049}}e^{\frac{-t\left(-\frac{4\pi^2\lambda_{11}}{a^2}-\frac{4\pi^2\lambda_{22}}{b^2}-\frac{\left(57+\sqrt{2049}\right)\lambda_{33}}{h^2}\right)}{4\rho c_v}}\left(4\left(\left(\left(33+\sqrt{2049}\right)hc_1+120c_0+e^{\frac{\sqrt{2049}t\lambda_{33}}{2h^2\rho c_v}}\right.\right.\right. \tag{F.3}$$

$$\left.\left.\left(\left(-33+\sqrt{2049}\right)c_1+120c_0\right)\frac{1}{h}\right)+\left(\sqrt{2049}\,e^{\frac{t\left(\frac{4\pi^2\lambda_{11}}{a^2}+\frac{4\pi^2\lambda_{22}}{b^2}+\frac{\left(57+\sqrt{2049}\right)\lambda_{33}}{h^2}\right)}{4\rho c_v}}\left(-3h^4\pi^4q^*\left(b^2\lambda_{11}+a^2\lambda_{22}\right)^2\right.\right.\right.$$

$$-2h^2\pi^2\left(b^2\lambda_{11}+a^2\lambda_{22}\right)\left(-41a^2b^2q^*+6h\pi^2T^*\left(b^2\lambda_{11}+a^2\lambda_{22}\right)\right)\lambda_{33}+48a^2b^2\left(25a^2b^2q^*\right.$$

$$\left.\left.\left.+11h\pi^2T^*\left(b^2\lambda_{11}+a^2\lambda_{22}\right)\right)\lambda_{33}^2\right)\right)/\left(\lambda_{33}\left(2h^4\pi^4\left(b^2\lambda_{11}+a^2\lambda_{22}\right)^2+57a^2b^2h^2\pi^2\right.\right.$$

$$\left.\left.\left.\left(b^2\lambda_{11}+a^2\lambda_{22}\right)\lambda_{33}+150a^4b^4\lambda_{33}^2\right)\right)\right)$$

where constants c_0 and c_1, particularized for $T_{R0}(0)=0$ and $T_{R1}(0)=0$, assume the expressions:

$$
\begin{aligned}
c_0 = &\left(-q^*\left(2h^5\pi^4\left(b^2\lambda_{11}+a^2\lambda_{22}\right)^2+15a^2b^2h^3\pi^2\left(b^2\lambda_{11}+a^2\lambda_{22}\right)\lambda_{33}-1800a^4b^4h\lambda_{33}^2\right)\right.\\
&\left.+T^*\left(-12h^4\pi^4\left(b^2\lambda_{11}+a^2\lambda_{22}\right)^2\lambda_{33}+90a^2b^2h^2\pi^2\left(b^2\lambda_{11}+a^2\lambda_{22}\right)\lambda_{33}^2+3600a^4b^4\lambda_{33}^3\right)\right)/\\
&\left(24\lambda_{33}\left(2h^4\pi^4\left(b^2\lambda_{11}+a^2\lambda_{22}\right)^2+57a^2b^2h^2\pi^2\left(b^2\lambda_{11}+a^2\lambda_{22}\right)\lambda_{33}+150a^4b^4\lambda_{33}^2\right)\right)\\
c_1 = &\left(q^*\left(3h^4\pi^4\left(b^2\lambda_{11}+a^2\lambda_{22}\right)^2-82a^2b^2h^2\pi^2\left(b^2\lambda_{11}+a^2\lambda_{22}\right)\lambda_{33}-1200a^4b^4h\lambda_{33}^2\right)\right.\\
&\left.+T^*\left(12h^3\pi^4\left(b^2\lambda_{11}+a^2\lambda_{22}\right)^2\lambda_{33}-528a^2b^2h\pi^2\left(b^2\lambda_{11}+a^2\lambda_{22}\right)\lambda_{33}^2\right)\right)/\\
&\left(8\lambda_{33}\left(2h^4\pi^4\left(b^2\lambda_{11}+a^2\lambda_{22}\right)^2+57a^2b^2h^2\pi^2\left(b^2\lambda_{11}+a^2\lambda_{22}\right)\lambda_{33}+150a^4b^4\lambda_{33}^2\right)\right)
\end{aligned}
\tag{F.4}
$$

Eqs.(F.4) are also solutions of Eq.(15a,b) without source terms.

G. Case 3 (Sect.4.3): exact closed form non-stationary solution of Eqs. (2) in terms of temperature

By expressing Eqs.(4) in terms of configuration for this case, eliminating thermomechanical contributions, we have [32]:

$$
\begin{aligned}
&\left(2h^2H\lambda_{11}+12h\lambda_{11}\lambda_{33}\right)\frac{\partial^2T_0}{\partial^2x}+\left(2h^2H\lambda_{22}+12h\lambda_{22}\lambda_{33}\right)\frac{\partial^2T_0}{\partial^2y}-\left(2h^2H\rho c_v+12h\rho c_v\lambda_{33}\right)\frac{\partial T_0}{\partial t}\\
&-\left(24H\lambda_{33}\right)T_0+3(hH+4\lambda_{33})E^{(0)}=0\\
&\left(h^4H\lambda_{11}+12h^3\lambda_{11}\lambda_{33}\right)\frac{\partial^2T_1}{\partial^2x}+\left(h^4H\lambda_{11}+12h^3\lambda_{11}\lambda_{33}\right)\frac{\partial^2T_1}{\partial^2y}-\left(h^4H\lambda_{11}\rho c_v+12h^3\lambda_{11}\lambda_{33}\rho c_v\right)\frac{\partial T_1}{\partial t}\\
&-\left(60h^2H\lambda_{33}+120h\lambda_{33}^2\right)T_1+30(hH+6\lambda_{33})E^{(1)}=0
\end{aligned}
\tag{G.1}
$$

This equations are satisfied by the following solutions:

$$
T_0(x,y,t)=T_{R0}(t)\sin\frac{\pi x}{a}\sin\frac{\pi y}{b},\qquad T_1(x,y,t)=T_{R1}(t)\sin\frac{\pi x}{a}\sin\frac{\pi y}{b}
\tag{G.2}
$$

with

$$
T_{R0}(t)=c_0e^{-\frac{\left(\pi^2\left(\frac{\lambda_{11}}{a^2}+\frac{\lambda_{22}}{b^2}\right)+\frac{12H\lambda_{33}}{h^2H+6h\lambda_{33}}\right)}{\rho c_v}t}+\frac{3a^2b^2(hH+4\lambda_{33})E^{(0)}}{2b^2h\pi^2\lambda_{11}(hH+6\lambda_{33})+2a^2\left(12b^2H\lambda_{33}+h\pi^2\lambda_{22}(hH+6\lambda_{33})\right)},
$$

$$T_{R1}(t) = c_1 e^{-\frac{\left(b^2h^2\pi^2\lambda_{11}+a^2h^2\pi^2\lambda_{22}\right)(hH+12\lambda_{33})+a^2\left(60b^2\lambda_{33}(hH+2\lambda_{33})\right)}{a^2b^2h^2\rho c_v(hH+12\lambda_{33})}t} + \frac{30a^2b^2\left(hH+6\lambda_{33}\right)E^{(1)}}{h^3\pi^2\left(b^2\lambda_{11}+a^2\lambda_{22}\right)(hH+12\lambda_{33})+a^2h\left(60b^2\lambda_{33}(hH+2\lambda_{33})\right)} \tag{G.3}$$

where constants c_0 and c_1, particularized for $T_{R0}(0)=0$ and $T_{R1}(0)=0$, assume the expressions:

$$c_0 = \frac{3\,a^2b^2\left(h\,H+4\,\lambda_{33}\right)E^{(0)}}{2\left(b^2h\pi^2\lambda_{11}\left(h\,H+6\,\lambda_{33}\right)+a^2\left(12\,b^2H\,\lambda_{33}+h\,\pi^2\lambda_{22}\left(h\,H+6\,\lambda_{33}\right)\right)\right)}$$

$$c_1 = \frac{30\,a^2b^2\left(h\,H+6\,\lambda_{33}\right)E^{(1)}}{h\left(b^2h^2\pi^2\lambda_{11}\left(h\,H+12\,\lambda_{33}\right)+a^2\left(60\,b^2\lambda_{33}\left(h\,H+2\lambda_{33}\right)+h^2\pi^2\lambda_{22}\left(h\,H+12\lambda_{33}\right)\right)\right)} \tag{G.4}$$

Eqs.(G.4) are also solutions of Eq.(20a,b).